

**Far-Infrared Spectroscopy of M 82:
Interstellar Properties of the Dual Nuclear
Starbursts**

S. D. LORD^{1,2}, D. J. HOLLENBACH², M. R. HAAS², R. H. RUBIN^{2,3}

S. W. J. COLGAN^{2,4} AND E. F. ERICKSON²

¹IPAC, M/S 100-22, Caltech, Pasadena CA 91125

²NASA/Ames Research Center, MS 245-6, Moffett Field CA 94035

³Orion Enterprises

⁴SETI Institute

Draft Date: October 12, 1995

Submitted: October 13, 1995

ABSTRACT

We have measured $[\text{O I}] 63 \mu\text{m}$ and $[\text{Si II}] 35 \mu\text{m}$ in the central $44''$ (700 pc) of the starburst galaxy M82. The luminosities in these transitions are each $\sim 0.1\%$ of the bolometric luminosity. We model the $[\text{O I}]$ in M82 as arising from warm neutral gas photodissociated by FUV flux from OB stars, while most of the $[\text{Si II}]$ emission arises from associated H II regions. The gas phase Si/H abundance ratio is found to be $\sim 1.5 \times 10^{-5}$ about 3 times greater than that seen in galactic nebulae, where silicon is mostly bound up in grains. The enrichment is probably causal by the partial destruction of silicate grains by fast supernovae-driven SNIICs.

The $[\text{O I}] 63 \mu\text{m}$ and the $[\text{Si II}] 35 \mu\text{m}$ spectrum both show an asymmetric line profile indistinguishable in shape from those of the $[\text{O III}] 52$ and $88 \mu\text{m}$ and $[\text{N III}] 57 \mu\text{m}$ lines measured previously in M82. We detect two distinct velocity components, which we attribute to emission from two regions associated with the molecular gas concentrations located 190 pc ($1.2''$) on either side of the nucleus.

We separately model the two emission lobes and derive the cloud conditions in these two regions. The derived properties suggest that the clouds in these lobes are small, $r_{\text{cl}} \sim 0.4\text{--}1.0 \text{ pc}$, have warm, $T \sim 230 \text{ K}$, neutral gas surfaces, and are concentrated with volume filling factors of ~ 0.1 and area filling factors of $\sim 7\text{--}20$. Together, the two lobes, each of diameter $\sim 125 \text{ pc}$ ($\sim 8''$) are characterized by a large number, $\sim 3 \times 10^5$, of $\sim 600 M_{\odot}$ clouds with surface gas densities of $\sim 104 \text{ cm}^{-3}$ and with pressures of $P/k \sim 3 \times 10^6 \text{ cm}^{-3} \text{ K}$, illuminated by FUV fluxes $\sim 10^3$ times the average local interstellar value for the Milky Way. These highly pressurized clouds are held in pressure equilibrium by the surrounding H II regions and the hot intercloud medium. The clouds cannot long sustain the nuclear starburst. The intense FUV fluxes have already photodissociated about 10% of the molecular gas, and the combined effects of fragmentation, photoionization and photodissociation caused

by the massive stars will soon **destroy the** natal molecular environment.

Subject heading: galaxies: abundances - galaxies: individual (M82) galaxies: ISM

- galaxies: nuclei galaxies: starburst - infrared: galaxies

In the central regions, the gas responds to the presence of both an inner-ILRs⁶ and an⁹ outer-IL¹¹ by forming a ring of material at radii between the two ILRs. In M 82, at radii within 160 pc (10"), a ring of ionized gas has been¹ recently been mapped with high spatial and spectral resolution in observations of Br γ (Larkin et al. 1994) and [Nc II] 12.8 μ m (Achtermann & Lacy 1995).

The high concentrations of molecular gas give rise to a high star formation and supernova rates. Interferometric radio observations in the central region indicate that a supernova occurs about every 10-20 years (Muxlow et al. 1994, Ulvestad & Antonucci 1994, van Buren & Greenhouse 1994) and suggest an enormous starburst in which 106 early type stars ($M \sim 10 M_{\odot}$) were formed in the last $1 - 2 \times 10^7$ years. These stars provide the bulk of the continuum luminosity reradiated in the IR by the dust. Assuming a Miller-Scalo IMF (Miller & Scalo 1979), the current rate of supernovae and the infrared luminosity each imply a star formation rate of $1 M_{\odot} \text{ yr}^{-1}$, which would deplete the observed molecular gas in 2×10^8 years (hence, a "starburst"). The high supernova rate fuels a biconical wind of velocity $\sim 300 \text{ km s}^{-1}$ emerging normal to the torus (Heckman, Armus, & Miley 1990; Chevalier & Clegg 1985). The UV and shock heating and ionization from these stars and supernovae make the obscured central region of M82 ($A_V = 25 - 30$; see Puxley 1991, McLeod et al. 1993) a prime source for far-infrared (FIR) fine structure emission. Such emission is copiously produced in shocks (Hollenbach & McKee 1989), photodissociation regions (PDRs) (Tielens & Hollenbach 1985a (1985), Hollenbach, Takahashi, & Tielens

1990 (H T T)), and 1111 regions (Rubin et al. 1988). Observations at FIR wavelengths allow us to probe conditions within the opaque dusty centers

The mid- and far-infrared lines which have been measured in M82 to date are listed in Table 1, and Table 2 provides a summary of additional observations of the neutral and molecular gas. The observations of the H II gas can be summarized as follows. Beck et al. (1978) mapped the central region in [Ne II] 13 μ m, and found the presence of non-circular motions in the ionized gas and an approximately solar abundance for neon. Since neon is not expected to be significantly incorporated into grains, this gas phase measurement indicates nearly solar metallicities in the central regions of M82 (LeVan & Price 1987; Achtermann & Lacy 1995). By comparing the [S III] 19, 33 μ m lines and [O III] 52, 88 μ m lines, Houck et al. (1984) and Duffy et al. (1987) obtained a mean electron density for the central region of $n_e \sim 200 \text{ cm}^{-3}$, and ruled out the presence of a significant higher density ($n_e \gtrsim 10^3 \text{ cm}^{-3}$) component. The deduced thermal pressure in the H II regions is about $P/k \gtrsim 4 \times 10^6 \text{ cm}^{-3} \text{ K}$, three orders of magnitude higher than the average local (Milky Way) interstellar value, but similar to the pressures in Milky Way H II regions near OB stars. The high resolution [O III] 52, 88 μ m and [N III] 57 μ m profiles of Duffy et al. (1987) show virtually identical line shapes with a prominent peak at $\sim 130 \text{ km s}^{-1}$, blue-shifted by $\sim 90 \text{ km s}^{-1}$ with respect to the systemic velocity of M82. Duffy et al. suggested that the profiles owe their characteristic shape to the two 10 μ m hot spots (e.g., see Telesco & Gezari 1992) located on either side of the nucleus. They deduced a total

ionized gas mass of $4 \times 10^7 M_{\odot}$. The measured $[\text{O III}] 52 \mu\text{m}/\text{Br}\alpha$ ratio indicated a maximum stellar effective temperature of 35,000 K. The $\text{Br}\alpha$ luminosity indicates a Lyman continuum luminosity of $\sim 6 \times 10^{53}$ photons s^{-1} in the nucleus (cf. Carlstrom and Kronberg 1991), more than twice that of the *entire* Milky Way galaxy (Güsten and Mezger 1983). Roughly 10^5 massive O stars are required to provide the necessary excitation in the central 400 pc of M 82.

Previous observations of the FIR, emission from gas in the central region have led to some confusion about its distribution. In a study of the $[\text{O II}] 52, 88 \mu\text{m}$, $[\text{O I}] 63, 146 \mu\text{m}$, and $[\text{C II}] 158 \mu\text{m}$ lines, Lugten et al. (1986) decomposed the line profiles into two components: a broad feature spanning the entire 350 km s^{-1} range of the line, and the 130 km s^{-1} feature. The narrow feature had first been observed in $[\text{O I}] 63 \mu\text{m}$ by Watson et al. (1984), who suggested a possible shock origin. Lugten et al. found the $[\text{C I}] 1 \mu\text{m}$ emission spatially extended along the major and minor axes, and concluded that the blue-shifted feature originated from a location within $10''$ of the nucleus. They suggested that the emission might be associated with the SNR (41.9+W3). A remarkable result of the Lugten et al. study was that the $[\text{O I}] 63 \mu\text{m}$ profile showed significant emission at negative (and therefore peculiar) velocities. Seaquist, Bell, & Bignell (1985) speculated that the $[\text{O I}]$ emission at these peculiar velocities may be due to shock-heated neutral gas. However, in this work, we find no significant $[\text{O I}]$ emission at negative velocities and we propose a PDR or H II region origin for all of the observed emission. Assuming a PDR origin for the $[\text{O II}]$ and $[\text{C II}]$

emission, Lugten et al. found the atomic **density** to be $2 \times 10^4 \text{ cm}^{-3}$, the pressure to be $P/k \sim 2 - 6 \times 10^6 \text{ cm}^{-3} \text{ K}$, the atomic gas volume filling **factors** to be $\sim 10^{-3}$ in the central kiloparsec, and the neutral gas residing in small **clouds** less than a few pc in size.

In §2 we present new observations of the [O I] $63.184 \mu\text{m}$ line and the first published detection of the [Si II] $34.814 \mu\text{m}$ line from M82 (we note, however, that P. Graf (1988) lists a detection of [Si II] in M82 with a flux consistent with ours in his thesis). We address the *physical origin* of the emission in §3 and conclude that PDRs are responsible for the [O I] and [C II] emission, while H II regions are **probably** responsible for most of the [Si II] $35 \mu\text{m}$ emission. In §4 we examine the detailed *spatial origin* of the emission within the central region. To do this, we use multi-aperture spectra (§4.1) and kinematic arguments (§4.2) to constrain the location of the emission. Using the [O I], [C II], CO, and FIR continuum measurements, we determine in §5 the *physical conditions* of the warm interstellar gas and molecular clouds in the central 400 pc of M82. We summarize our results in §6.

2. OBSERVATIONS AND MODEL INDEPENDENT RESULTS

2.1. Data Acquisition and Calibration

The observations were made in 1986, 1987, and 1990 using the Cryogenic Grating Spectrometer on the Kuiper Airborne Observatory. The [O I] spectra observed with a $44''$ aperture required significant corrections for atmospheric absorption on

the red-shifted side of the observed profiles (see Figure 1) where the absorption at 650 km s^{-1} is nearly 100%. The [Si II] line was observed with both 34" and 44" apertures; the atmospheric absorption is less than 1% across this waveband. The details of the data reduction are given in Appendix A, and involve wavelength calibration, flux calibration, and removal of systematic offsets. Reduced [O I] and [Si II] spectra are shown together in Figure 2 where the similarity of the two profiles is evident. In these spectra, the overlapping data from different echelle grating settings produce nonuniformly spaced points, each with a spectral resolution of 106 km s^{-1} for [O I] and 81 km s^{-1} for [Si II]. The error bars shown are 1σ statistical values.

2.2. Model-Independent Results

The observed line and continuum fluxes and intensities and the derived luminosities are given in Table 3. From the line luminosities, we can derive several model-independent results. No significant [O I] $63 \mu\text{m}$ emission can originate in H II regions since the neutral oxygen abundance in H II regions is extremely small (e.g., Rubin 1985). Regardless of whether the [O I] $63 \mu\text{m}$ emission originates in PDRs, shocks, or X-ray heated neutral gas, we are able to estimate the *minimum* total mass of associated neutral gas M_H from the [O I] luminosity by assuming LTE, and by assuming that all oxygen exists in the atomic state and that the gas temperatures are higher than the [O I] $63 \mu\text{m}$ excitation temperature ($T \gg \Delta E/k = 228 \text{ K}$):

$$M_H \geq 3 \times 10^5 \left[\frac{L_{\text{OI}}}{5.4 \times 10^7 L_\odot} \right] \left[\frac{6 \times 10^{-4}}{x_O} \right] M_\odot, \quad (2.1)$$

where x_O is the gas phase oxygen abundance relative to hydrogen.

Likewise, regardless of the origin of the [Si I 1] emission, we can estimate the minimum total associated gas mass from the [Si II] luminosity by assuming LTE, and by assuming that all the silicon is singly ionized form and $T \gg 413$ K:

$$M_H \geq 6 \times 10^5 \left[\frac{L_{\text{SiII}}}{4.5 \times 10^7 L_\odot} \right] \left[\frac{3 \times 10^{-5}}{x_{\text{Si}}} \right] M_\odot, \quad (2.2)$$

where x_{Si} is the gas phase abundance of silicon. We shall argue below that [Si II] likely originates in H II regions, so M_H derived from the silicon refers to the minimum ionized H II gas mass.

With the minimal assumptions of a solar C/O abundance ratio, optically thin emission, and spatially coincident [C II] and [O I] regions, a temperature estimate can be derived from the flux ratio [C II] 158 μm /[O I] 63 μm = 1.1. For neutral gas densities in the range $n \sim 10^3 - 10^5 \text{ cm}^{-3}$, this ratio implies $T \sim 200 - 500$ K (see Figure 3 of TII). These gas temperatures and densities are similar to dense PDRs associated with massive stars in the Milky Way Galaxy (Hollenbach & Tielens 1995).

3. PHYSICAL ORIGIN OF THE [O I] 63 μm , [C II] 158 μm , AND [Si II] 35 μm EMISSION IN M 82

The [O I] 63 μm , [C II] 158 μm , and [Si II] 35 μm emission may be produced variously in the warm atomic gas behind dissociative shocks (see Werner et al. 1984; Haas et al. 1986; Hollenbach & McKee 1989), in X-ray heated gas (Draine & Woods 1990), in H II regions (Rubin et al. 1985), or in PDRs (TII; Sternberg & Dalgarno

1989; 11'1"1'; Burton, Hollenbach & Tielens 1990). In this section, we argue that in the central 400 pc of M82 the [O I] and most of the [C II] emission originates in PDRs. H II regions may, however, be responsible for a major fraction of the [Si II] emission and a minor component of the [C II] emission.

3.1. Shock Waves from Stellar Winds Versus PDRs

Although winds from early type stars or protostars likely generate numerous shocks in the central kpc of M 82, a simple energy argument demonstrates that the resultant fine structure luminosity from these shocks is insignificant compared to the emission from PDRs. Consider an early type star with luminosity L : the energy radiated in its lifetime is $10^{53} L_5 t_7$ ergs, where $L_5 = L/10^5 L_\odot$ and $t_7 = t/10^7$ years is the main sequence lifetime. Typically, for OB stars, $L_5 t_7 \sim 1$ (Tutukov & Krugel 1981). We show that in PDRs powered by OB stars, $\epsilon \sim 10^{-3} - 10^{-2}$ of this radiated bolometric energy is converted to [C II] 158 μm + [O I] 63 μm line emission if the stellar radiation is absorbed by dust. Thus, the energy E_{PDR} radiated in these lines over the lifetime of the star is

$$E_{\text{PDR}} = 10^{50} \epsilon_{-3} L_5 t_7 \text{ ergs}, \quad (3.1)$$

where $\epsilon_{-3} = \epsilon/10^{-3}$ is the efficiency of converting starlight to line cooling in these FIR transitions. On the other hand, the total kinetic energy in ejected wind material is

$$E_w = \int \frac{1}{2} \dot{M}(t) v_w^2(t) dt, \quad (3.2)$$

where \dot{M} is the mass loss rate and v_w is the wind velocity. Assuming that the star loses approximately equal amounts of mass in the protostellar, main-sequence, and post main-sequence (supergiant) phases, then the energetics are dominated by the main-sequence phase because of the considerably higher wind speeds during this phase. Thus,

$$E_w = 10^{49} M_{ej} v_{w8}^2 \text{ ergs}, \quad (3.3)$$

where M_{ej} is the mass ejected in solar masses during the main-sequence phase and v_{w8} is the wind velocity in units of 1000 km s^{-1} . Typically, for OB stars, $M_{ej} v_{w8}^2 \sim 1$ (van Buren 1985). Thus, even if all the wind mechanical energy were radiated in the shocks via [C II] $158 \mu\text{m}$, [O I] $63 \mu\text{m}$, and [Si II] $35 \mu\text{m}$, the PDR emission still dominates the shock emission by a factor of order 10–100. In fact, only a fraction of order $10^{-2} v_{w8}^{-1}$ of the wind energy is radiated in these lines (see Hollenbach & McKee 1989). Thus, for a given early type star, the ratio of the PDR emission to the shock emission (in [C II], [O I], and [Si II]) is of order

$$\frac{E_{\text{PDR}}}{E_{\text{shock}}} = 10^3 \left(\frac{\epsilon_{\text{PDR}}}{M_{ej} v_{w8}} \right), \quad (3.4)$$

averaged over the lifetime of the star, where the factor in parenthesis is of order unity.

Observations of Orion A, where both shocks (Werner et al. 1984) and PDR emission (Stacey et al. 1993) have been observed, bear out the dominance of the PDR component. The observed PDR luminosity in [C II] $158 \mu\text{m}$ + [O I] $63 \mu\text{m}$ + [Si II] $35 \mu\text{m}$ $\gtrsim 2 \times 10^3 L_{\odot}$, whereas the very powerful and short-lived shock emission is $\simeq 50 L_{\odot}$ in these same lines. The instantaneous ratio $E_{\text{PDR}}/E_{\text{shock}}$ is 40, but the ratio

averaged over the 10^7 year lifetime of the PDR becomes much larger (see Eq. 3.4).

3.2. Shocks and X-Rays from Supernovae Versus PDRs

Although stellar winds are energetically unfavorable, we cannot rule out supernova shock emission or emission from gas heated by X-rays from supernovae shocks with an energy argument. The kinetic energy in the supernova of an OB star is $E_{\text{SN}} = 10^{51} E_{51}$ ergs, where E_{51} is of order unity. The fraction of that energy radiated by the fine structure lines in associated shocks is of order $0.1 v_7^{-1}$, where v_7 is the critical velocity, in units of 100 km s⁻¹, at which the supernova shock becomes radiative (Hollenbach & McKee 1989). Thus, over the lifetime of an early type star, the ratio of fine structure energy emitted by PDRs to fine structure energy emitted by shocks driven by the final supernova of the star is

$$\frac{E_{\text{PDR}}}{E_{\text{SN}}} \approx \frac{\epsilon_{\text{F}} 3 I_5 t_7 v_7}{E_{51}}. \quad (3.5)$$

This factor is sufficiently close to unity that supernova shocks cannot be ruled out as the dominant origin of the fine structure emission. In fact, a somewhat more direct argument reinforces this conclusion. The inferred current supernova rate in the central kpc of M82 (0.05 per year; Ulvestad & Antonucci 1994), implies a current mechanical luminosity in supernova ejecta of $4 \times 10^8 L_{\odot}$, a factor of about 4 greater than the observed luminosity in [C II] 158 μm + [O I] 63 μm + [Si II] 35 μm . Thus, the shock luminosity is negligible only if the fraction of the ejecta energy radiated by these lines is appreciably less than ~ 0.25 .

Likewise, supernovae generally convert a **big** fraction of their 10^{51} ergs of kinetic energy into X-rays, and the resulting X-rays penetrate surrounding neutral gas and heat the gas with efficiencies of order 0.1-1.0 (see Draine & Woods 1990). Therefore, we cannot rule out shocks or X-rays from supernovae with simple energetic arguments and we must **turn** to other discriminants between these heating sources and PDR heating. We discuss four such discriminants below.

Hollenbach & McKee (1989) give diagnostics which are helpful in distinguishing between shocks, PDRs, and X-ray heated gas. The first involves the ratio of $[\text{O I}] 63 \mu\text{m}/[\text{C II}] 158 \mu\text{m}$ and the absolute intensity of $[\text{O I}] 63 \mu\text{m}$. Ratios $\gtrsim 10$ along with absolute $[\text{O I}]$ intensities $\gtrsim 10^{-4} \text{ erg cm}^{-2} \text{ s}^{-1} \text{ sr}^{-1}$ are characteristic of **shock** emission, whereas PDRs with high absolute $[\text{O I}]$ intensities **produce** ratios less than 10. These intensities are constrained in **this** manner because shocks tend to **produce** less column density of warm atomic gas **than** PDRs or X-ray heated gas. Therefore **shocks** must have higher temperatures and densities than PDRs or X-ray heated gas to produce equivalent $[\text{O I}]$ intensity. At high densities and temperatures, $[\text{O I}] 63 \mu\text{m}/[\text{C II}] 158 \mu\text{m} > 10$. In M82 a **relatively low** $[\text{O I}]/[\text{C II}]$ ratio of ~ 1 is observed over the entire central (~ 700 pc) region, indicating a PDR or X-ray heated origin for the $[\text{O I}]$ emission. An identical argument implies the $[\text{Si II}]$ emission **also** does not originate from shocks.

A second diagnostic between PDRs, X-ray heated gas, and shocks is the ratio $([\text{C II}] 158 \mu\text{m} + [\text{O I}] 63 \mu\text{m})/\text{total IR luminosity}$. As discussed by TII, Hollenbach

(1990), and Wolfire, Tielens, & Hollenbach (1990, hereafter WTH), this ratio is theoretically predicted and observed to be of order 10^{-3} to 10^{-2} in PDRs illuminated by OB stars. However, in shocks this ratio is unconstrained and depends on such variables as the shock velocity and preshock density. Likewise, in X-ray heated gas, Maloney et al. (1995) find a large range for this ratio, depending on the X-ray flux and gas density. Therefore, the observation in M82 of a ratio $\sim 2 \times 10^{-3}$ (see Tables 2 and 3) is more naturally explained with a PDR origin for the [C II] and [O I] emission.

A third form of evidence for a PDR origin of the [C II] line in M82 is given by the observations of Crawford et al. (1985) of the correlation of [C II] $158 \mu\text{m}$ to CO ($J=1-0$) towards regions (including the nucleus of M82) of high FUV fields and the subsequent interpretation of the correlation by Wolfire, Hollenbach & Tielens (1989) and Stacey et al. (1991). These groups modeled the correlation in terms of FUV illuminated molecular clouds in which the [C II] $158 \mu\text{m}$ is produced near the surface and the CO ($J=1-0$) somewhat deeper into the cloud. The fact that M82 follows the same correlation as well-studied PDR regions in our own galaxy lends support to the supposition that much of the [C II] $158 \mu\text{m}$ fine structure emission in M82 arises predominantly in the PDR surfaces of a large ensemble of molecular clouds.

Finally, the close correlation between the line profiles of [O III] $52 \mu\text{m}$, $88 \mu\text{m}$ and [N II] $57 \mu\text{m}$ (Duffy et al. 1987) with the [O I] $63 \mu\text{m}$ profile is naturally explained if [O I] originates in photodissociated gas which is adjacent to, and travels with the orbiting H II regions. Supernova shocks, on the other hand, would not necessarily

correlate with the dense H II regions (see, for example, Telesco & Gezari 1992, who find no obvious correlation of supernova remnants and H II regions in M 82), and the supersonic velocities would alter the line profile relative to the profiles from the H II plasma,

3.3. H II Regions

The ionization balance in H II regions results in some C^+ , O^0 , and Si^+ in the H II plasma which will contribute to the fine structure emission. Because O^0 has an ionization potential similar to H and a rapid charge exchange reaction proceeds between the two species, the O^+ / O^0 ratio is nearly identical to the H^+ / H ratio in H II regions. Therefore, the O^0 abundance in H II regions is extremely low and the $[O I] 63 \mu m$ contribution is insignificant.

However, the contribution of $[C II] 158 \mu m$ and $[Si II] 35 \mu m$ from the H II regions produced by the $\sim 10^5$ O stars in the central region of M 82 may be significant. Figure 3 displays the results of applying the Rubin (1985) H II region code to a simple model of 60,000 O stars, each with Lyman continuum luminosity of $N_{LyC} = 10^{49}$ photons s^{-1} and each embedded in a constant density, $n_e = 190 \text{ cm}^{-3}$, ionization-bounded H II region. The observed values are shown with filled circles and 1σ error bars while the model values are open squares. Extinction corrections for wavelengths shorter than $35 \mu m$ are significant, with $\exp(\tau)$ ranging between 1.3 and 2.2. Most of the model values in this short wavelength range are within 10% of the observations. The relatively poorer fit to $[Ne II]$ (the model assumes solar abundance for gas phase

neon, see below) may be attributed to the large and uncertain extinction correction applied for this short wavelength line. The model fits the data well at the longer wavelength transitions, with the exception of the [C II] and [Si II] lines, which the model underpredicts; however, the model [C II] and [Si II] line fluxes are proportional to the assumed gas phase abundances of C and Si, respectively. Figure 3 assumes $[C/H] = 2.8 \times 10^{-4}$ and $[Si/H] = 4.5 \times 10^{-6}$ (85% of the silicon is in grains), values appropriate for diffuse clouds and H II regions in the solar vicinity (Rubin, Dufour, & Walter 1993). Thus, a gas phase [C/H] ratio of $\sim 10^{-3}$ and [Si/H] ratio of 1.5×10^{-5} are required for H II regions to produce the bulk of the observed [C II] $158 \mu\text{m}$ and [Si II] $35 \mu\text{m}$ emission.

The [Si II] $35 \mu\text{m}$ emission can originate from H II regions if the elemental silicon abundance in M 82 is solar and only 50% of the silicon is in grains, as might result from the supernova shock destruction of dust in the M82 nucleus. Alternatively, the [Si II] $35 \mu\text{m}$ emission could originate in H II regions if the elemental silicon abundance were about 5 times solar, and a “solar neighborhood” 85% of the silicon was incorporated in dust. Beck et al. (1978) describe [Ne II] $13 \mu\text{m}$ observations which suggest roughly solar abundances of heavy elements in M82. Therefore, if H II regions produce most of the [Si II] emission, we favor a model with solar *elemental* abundances of Si, but only one half the Si bound in grains and a *gas phase* silicon abundance of $\sim 1.5 \times 10^{-5}$.

Solar elemental abundances mean, however, that only $\leq 30\%$ of the [C II] $158 \mu\text{m}$ emission originates in H II gas. Carral et al. (1994) compare the [C II]

emission from an ionization-bounded H II region with the [C I 1] emission from the PDR which surrounds the ionized gas. They show that, regardless of the elemental abundance of C, the PDR dominates the C I emission (by factors of typically 2-3) as long as $n_e \gtrsim 10 \text{ cm}^{-3}$ in the H II region and T_{eff} of the central star exceeds 33,000 K. We conclude that $\lesssim 30\%$ of the [C II] emission is produced in H II gas and that most originates in PDRs.

3.4. The Origin of the [Si II] 35 μm Emission

We have suggested that an H II region origin for [Si II] 35 μm is possible with high silicon gas phase abundances. We must now examine PDR contributions in the high-abundance case, and determine whether PDRs could dominate the total [Si II] 35 μm emission. The observed [Si II] 35 μm luminosity in M82 is nearly the same as the [O I] 63 μm luminosity, whereas theoretical models of PDRs (TII) predict [Si II] 35 μm /[O I] 63 μm ratios of order $\lesssim 0.1[(x_{Si^{+}}/x_{O^0})/10^{-2}]$, where $x_{Si^{+}}$ and x_{O^0} are the gas phase abundances of Si^+ and O^0 , and 10^{-2} is the appropriate value of this abundance ratio in diffuse clouds (cf., Van Steenberg & Shull 1988). In diffuse clouds, most of the elemental oxygen is in the gas phase whereas $\sim 85\%$ of the elemental silicon is tied up in dust. A [Si II] 35 μm /[O I] 63 μm ratio of order unity is also observed in the galactic center (Graf et al. 1988) and in M7 (Meixner et al. 1992), and in both cases a PDR origin has been invoked. Although the galactic center may be explained by high $x_{Si^{+}}/x_{O^0}$, such an explanation seems unlikely in M7 where we would expect silicon to be depleted as is observed in most diffuse and molecular

clouds. Meixner et al. (1992) suggest that the $[\text{Si II}] 35 \mu\text{m}/[\text{O I}] 63 \mu\text{m}$ ratio in M17 may be understood by assuming self absorption of the $[\text{O I}] 63 \mu\text{m}$ emission by cold foreground clouds. Additional self absorption of $[\text{O I}] 63 \mu\text{m}$ in M82 seems unlikely because the ensemble of clouds which produce the $[\text{O I}] 63 \mu\text{m}$ emission are orbiting at high velocities and the probability that one cloud absorbs line emission from another is very small.

Therefore, for $[\text{Si II}] 35 \mu\text{m}$ to have a PDR origin in M82, we require that the gas phase silicon abundance be high $x_{\text{Si}^+} \sim 3 \times 10^{-5}$ (solar) in the PDR. However, the gas phase silicon abundance in H II regions should be at least as high as the abundance in the neighboring PDRs. We have shown in §3.3 that a gas phase silicon abundance of $\sim 1.5 \times 10^{-5}$ will produce all the $[\text{Si II}] 35 \mu\text{m}$ emission in H II regions.

We conclude that the gas phase silicon abundance is high, $\sim 10^{-5}$, and that most of the $[\text{Si II}] 35 \mu\text{m}$ emission arises from the observed H II gas. Because the $[\text{Ne III}] 13 \mu\text{m}$ observations of the nucleus give little indication that the *elemental* abundance of the heavy elements are much higher than solar (Beck et al. 1978), it appears that the fraction of silicon in silicate grains is less than the diffuse ISM value of 0.85, presumably because of the vaporization of grains by supernova shocks in the violent central regions of M82. We have argued for a similar H II origin for $[\text{Si II}]$ in NGC 253 (Carral et al. 1994). We speculate that this may be a common situation in starburst nuclei.

4. Distribution of the Emitting Gas and Dust

4.1. Emission Distribution Inferred from Single Apertures

Tile many studies of the gas and dust in the center of M 82 show that the emission originates from an elongated structure, as from a bar or a disk of size $\sim 13 \times 26''$ or $\sim 200 \times 400$ pc (Joy, Lester, & Harvey 1987; Telesco et al. 1991; Telesco & Gezari 1992; Waller et al. 1992). Figure 4 shows contours for the nonthermal radio emission, the CO J= 1 - 0 emission, the H I (21 cm) emission, the dense molecular gas tracers such as CS, and the 30 μ m and 40 μ m dust emission. All these emission distributions show an elongated structure having the same inclination angle in the inner kpc. The most striking attribute of the many emission distributions seen in Figure 4 is that they do *not* peak at the nucleus, but rather show dual peaks in the Northeast and Southwest at distances of 5 - 15'' (75 - 225 pc) from the center. The occurrence of "twin peaks" of molecular emission¹⁵ is recognized as a common phenomenon in star burst galaxies, and may originate as products of inner Lindblad resonances (Kennedy et al. 1992, Telesco et al. 1991). An alternate possibility for the origin of these hot spots is from the edge-on viewing of a single tightly wrapped inner spiral arm (Telesco et al. 1991; Shen and Lo 1995).

The FIR line emission is consistent with an origin in an elongated or bilobal structure. One indication of this comes from comparing multi-aperture observations. In Figure 5 we plot the relative flux for the [O I] lines seen with a 30'' and 40'' aperture (Lugten et al. 1986), and for the [Si I 1] observations taken with a 34'' and a 44''

X

GH
a. or the

aperture (this work). The data show an increase in flux with aperture size consistent with an extended disk, represented here by the distribution of the $40\ \mu\text{m}$ continuum emission (dashed line), but inconsistent with an inner case in flux with aperture size from a uniform distribution (dotted line).

In contrast to the [O II] and [Si II] distribution, the [C II] $158\ \mu\text{m}$ emission, mapped by Lugten et al. (1986) and by Stacey et al. (1991) originates from a more extended region, with a similar but, larger disk-like distribution. The map of Stacey et al. shows [C II] emission with a FWHM along the major axis of $45''$, mostly unresolved emission along the minor axis, but with some [C II] emission as far as $2''$ from the center along the minor axis.

4.2. Separating the Northeast and Southwest Components

The [O I] and [Si II] line profiles have remarkably similar shapes, as may be seen in Figure 2. Each profile has a major peak at $v \sim 145\ \text{km s}^{-1}$ and a minor peak or shoulder at $v \sim 320\ \text{km s}^{-1}$. This same pattern is also seen in the [O III] $52\ \mu\text{m}$, [O III] $88, 111$, and [N III] $57\ \mu\text{m}$ line profiles (Duffy et al. 1987) and suggests that the emission seen in all of these lines originates in the same or closely associated regions.

We have fitted Gaussians with a flat continuum to the [O I] and [Si II] profiles with results given in Table 4 and Figures 6a, 1). Each fit used 6 free parameters: the height, width, and centroid for each of the two Gaussians. The reduced χ^2 for each fit is of order unity, indicating that the profiles are adequately fit by the functions. Table 4 shows that the velocity centroids and widths of the two Gaussians (each) for

the two lines match within the errors,

Just as the [C II] emission appears to be more extended than the [O I] and [Si II] emission, the shape of the central [C II] profile (Lugten et al. 1986) is also different from that of the [O I] and [Si II] profiles. It is more centrally peaked in velocity, and does not show a pronounced 320 km s^{-1} shoulder. However, we have preliminary data (Carral et al. 1996, in preparation) which seems to indicate a somewhat different central [C II] profile than that seen by Lugten et al. Therefore, rather than trying to apply a two Gaussian fit to the published [C II] data, we have elected to estimate the [C II] line flux in the two velocity components seen at other wavelengths by simply identifying velocity ranges for the two components. The fluxes in the [O I] and [Si II] Gaussian components are recovered if we identify as the northeast component the integrated emission for $v > 250 \text{ km s}^{-1}$ and as the southwest component, the integrated emission for $v < 250 \text{ km s}^{-1}$. The resultant [C II] fluxes for the two components are given in Table 3.

The velocity field of the inner kpc of *M82* can be used to deduce where the FIR line emission originates. We have examined the high resolution velocity field from $\text{H}\alpha$ (Heckathorn 1972; O’Connell & Mangano 1978), CO J=1–0 (Carlstrom 1988; Shen & Lo 1995), and [Ne II] (Achtermann & Lacy 1995). These velocity maps all show consistent trends in the central region. Within the inner 1 kpc, the line-of-sight velocities change most rapidly along the major axis passing through the center of the galaxy, as expected from rotation. The mean gas velocities taken from Carlstrom

(1988) run roughly linearly from 120 to 320 km s⁻¹ along the major axis from -10" in the southwest to 10" in the northeast. This same general rotation curve is apparent in the more highly resolved CO map of Shen & Lo (1995), and the [Ne II] map of Achtermann & Lacy (1995), but for these maps more velocity crowding is visible in the southwest. The H α field shows similarly spaced isovelocity contours running along the major axis, but with S-shaped distortions indicating streaming and/or z-motions (see Figure 4). Beyond 10" the velocities change more slowly, reaching 90 km s⁻¹ and 370 km s⁻¹ at $\pm 20''$ from the center, while maintaining a dispersion of 50-100 km s⁻¹. In the regions beyond $\pm 10''$, where the rotation curve flattens, there are many indicators of enhanced emission due to star formation.

The velocity centroids of the [O I] and [Si II] emission features indicate that the emission peaks originate at distances about 10" to the NE and SW of the nucleus. Figure 4 displays the H α isovelocity contours crossing the major axis in M 82 along with filled circles on the major axis positions with velocities matching the velocities of the [O I] and [Si II] peaks. We have placed the blue-shifted FIR line emission feature close to the nucleus, where there is a bright mid-infrared and Ne II peak. Because of the relatively flat rotation curve beyond this point, the red-shifted emission could also originate further from the center. A second plausible CO peak is located about 5" further southwest. Comparing these positions with the map of Shen & Lo (Figure 4, center left panel) we see that the northeast and southwest components have counterparts: Shen and Lo label these positions F2 and C1 and they are within

3" of the assumed PDR hot spot positions, Figure 7, panels (i) and (k). With the velocity crowding apparent in the map of Shen & 1,0 (1995), region W3, a third CO peak located about 15" southwest of the 2.2 μm center may also be part of the southwest hot spot.

To gauge the location and compactness of the FIR line emission in the northeast and southwest "hot spots," we have made sample synthetic line profiles using the detailed disk velocity fields. The synthetic spectra shown in Figure 7 were made using the $\text{H}\alpha$ field, and little variation was found if the CO ($J=1-0$) field was used instead. The synthetic profiles were generated from three input components: the velocity field, the emission distribution, and the instrument beam profile. A Gaussian velocity dispersion with $\sigma = 63 \text{ km s}^{-1}$ was used in each case, to match the major axis dispersion seen in the CO, $\text{H}\alpha$, and H I data. Emission distributions of dust, atoms and molecules were gathered from the literature (left panels, Figure 7). The CGS beam shape used for our [O I] and [Si I I] observations was simulated. These computer models yielded the synthetic "line" profiles (velocity histograms) seen in the right hand panels. Figure 7 (right panels) show that four assumed emission distributions (12 μm ; 40 μm ; 3 mm; and CO) result, in nearly Gaussian velocity distributions, with a median velocity near 200 km s^{-1} . The only models found to replicate the observed double-humped [O I] and [Si I I] profiles were those which assumed the emission to be confined to small ($< 8''$) regions on either side of the nucleus as shown in panel (i) and (ii). The hot spot model in panel (i) used an emission region $\sim 8''$ in diameter.

(FWHM) while the model shown in panel (k) used emission regions $2''$ in diameter. We prefer model (i) because of its closer correspondance to the CO distribution. The best fitting velocity dispersion in these models was found to be 60 km s^{-1} and 65 km s^{-1} respectively. When regions larger than $8''$ were considered, these could not be fit, because velocity dispersions which produced the correct overall line width failed to retain the double humped structure. Comparing the synthetic profiles to the observed [O I] profile, we conclude that the northeast and southwest components of the [O I] and [Si I] lines are separated by about $20''$, consistent with the bright CO peaks of Shen & Lo (1995). However, with extreme velocity crowding, the separation could range from $10''$ to $30''$. There does not appear to be an appreciable central component present.

What causes these two peaks? We suggest that the two FIR line emitting lobes represent either the cross-section of a molecular torus of emission or molecular gas concentrations located just exterior to an ionized gas torus, as depicted by Larkin et al. 1994. This proposal was first laid out by Telesco et al. (1991) and given observational support by Larkin et al. (1994) and Achtermann & Lacy (1995). The ionized ring is in direct contact with the molecular gas concentrations, which are located on either side of the central bar where the leading dust lane crosses the outer-ILR. The bar potential causes the orbits to crowd here. A good example of this morphology may be seen (face-on) in the galaxy NGC 6951 discussed by Kenney et al. 1992).

5. MODELING THE CENTRAL 400 PARSECS OF M82

5.1. PDR Modeling

Ensembles of clouds exposed to FUV radiation have been modeled by Wolfire, Tielens, & Hollenbach (1990; WTH). These authors show how to use IR and millimeter observation to derive parameters including the gas density n_a in the photodissociated cloud surfaces, the surface gas temperature T_a , the cloud area ϕ_a and volume ϕ_V filling factors, the incident FUV flux G_0 on each cloud, the average FUV flux in the ISM G_{AV} , and the number N_{cl} and radii r_{cl} of the clouds. The essence of the modeling is that line ratios give the density, temperature and incident, FUV flux on the clouds, line strengths give the atomic and molecular mass, and a comparison of the atomic mass with the molecular mass gives the number and size of the clouds, since greater numbers of small clouds result in more surface area and therefore in a higher atomic/molecular ratio. The parameters N_{cl} , r_{cl} , and ϕ_V are the most uncertain in the derivation, in part because they depend sensitively on an estimated value for the molecular gas mass and on an assumed value for η , the ratio of the density in the molecular center of each cloud to the surface atomic density. N_{cl} , r_{cl} , and ϕ_V also depend on the dimensions of the emitting region. To estimate the dimensions, we consider the 200×400 pc ($26 \times 13''$) region enclosed by the half power contour of the FIR continuum, as outlined by the $40 \mu\text{m}$ map of Joy et al. (1987), a size consistent with the detailed MIR map of Telesco & Gezari (1992). We

treat three different **spatial distributions within this region**. The most simple is a uniform emission distribution over the entire 200×400 pc region (**Model 1**). As a refinement, we divide the $40 \mu\text{m}$ continuum map into northeast and southwest components (along the major axis) with areas based on the FIR continuum contours (**Model 2**). Lastly, we consider the confined emitting **hot spots** implied by the analysis in §4.2. These regions are modeled as 125×125 pc ($8 \times 8''$) regions on either side of the nucleus (**Model 3**). **Model 3 is our preferred model**. The WTH procedure is described briefly in Appendix B.

In applying the WTH procedure to M82, we have used the improved molecular mass estimate of Wild et al. (1992), $M(\text{H}_2) = 1.8 \times 10^8 M_\odot$, derived from a multi-transitional and isotopic study (see Appendix C). In our models, we have assumed a core to surface density ratio $\eta = 3$, which represents a mean between a turbulence-dominated cloud ($\eta \sim 1$) and a cloud in thermal pressure equilibrium ($\eta \sim 10$, assuming $T_a \sim 300$ K and a molecular core temperature of ~ 30 K). We used the observed fluxes in the two velocity components to model the northeast and southwest regions separately. Since the Wild et al. molecular mass is larger than previous estimates which assumed optically thin CO emission (Appendix C), we have also run models with half the mass ($0.9 \times 10^8 M_\odot$) to examine our sensitivity to the molecular mass.

The results of the WTH analysis are shown in Table 5. The one-component (**Model 1**) results confirm the previous analysis of Lugten et al. (1986) and WTH,

which showed small, dense clouds illuminate by intense FUV fluxes. The two component models (2 and 3) show differences in the physical conditions in the northeast and southwest components. This can be intuitively understood by noting that the $[O I]/[C II]$ flux ratio in the northeast component is approximately 3 times larger than the ratio in the southwest component, and that this ratio increases with increasing gas density and temperature (TH). The model results suggest, that there are more clouds of lower mass $\sim 200 M_{\odot}$ in the southwest region, while in the northeast region the clouds are hotter and more massive $\sim 3000 M_{\odot}$ (the mass per cloud is obtained by dividing the total mass by the number of clouds). The area and volume filling factors are the only derived parameters which differ in Models 2 and 3, because the filling factors are calculated for different sized regions. However, the most striking general result is the large number ($\sim 10^5 - 10^6$) of small $r_{cl} \sim 0.4 - 1.0$ pc, $M_{cl} \sim 200 - 3000 M_{\odot}$ clouds which populate the nucleus. These clouds have surface gas densities of order 10^4 cm^{-3} , incident FUV fluxes $10^3 - 10^4$ times the local interstellar value, and surface temperature in the atomic gas of $\sim 200 - 300$ K. They are “separate” clouds in the sense that they do not appreciably shield each other from the FUV field; given this requirement, however, they may still be clustered to some extent, for example, in sheets, filaments or hot spots. This point is important enough to be reiterated: our modeling procedure basically compares the atomic mass to the molecular mass to determine the surface area of neutral cloud exposed to dissociating UV radiation. Therefore, we are not necessarily advocating an ensemble of spherical clouds of radius

r_{cl} , but r_{cl} represents the size scale (thickness or diameter) of the spherical, sheetlike, or filamentary neutral clouds which populate the nucleus.

The derived n_a and T_a in the PDRs give a thermal pressure of $\sim 3 \times 10^6 \text{ K cm}^{-3}$. This PDR pressure is comparable to the average thermal pressure in the M 82 II regions, $4 \times 10^6 \text{ K cm}^{-3}$ as modeled by Duffy et al. (1987) and Houck et al. (1984), which suggests that pressure equilibrium has been established between the PDRs and the presumably neighboring II regions.

The mass of the ionized gas can be calculated by comparing the thermal radio continuum (Carlstrom 1988) or the Br α luminosity (Willner et al. 1977) with the electron density $n_e \sim 200 \text{ cm}^{-3}$ determined from line ratios by Houck et al. (1984) and Duffy et al. (1987); the result is $M_{\text{I II}} \sim 1.2 \times 10^7 M_{\odot}$. The volume of the emitting gas is found by dividing $M_{\text{I II}}$ by the density; the result is $5 \times 10^{61} \text{ cm}^3$. The volume filling factor of the ionized gas is ~ 0.07 if we assume a disk of thickness 200 pc and diameter 400 pc, ~ 0.15 if it is a bar of diameter 200 pc ($1.3''$) and length 400 pc ($26''$), and unity if all the ionized emission originates from two hot spots (northeast and southwest) that are spheres with diameters 125 pc ($8''$) (Model 3).

The derived filling factors and densities of the neutral and ionized components suggests the small, dense, neutral clouds are embedded in volume significantly filled with II plasma, in a highly pressurized ISM ($\sim 10^3$ times the average pressure in the local Milky Way). Given its size of $\sim 0.5 \text{ pc}$ and surface temperature of 250 K, a single cloud has a dynamical (thermal) expansion timescale of $\lesssim 3 \times 10^5$ years.

In order for such **highly** pressurized neutral clouds and H II regions to persist, the *entire* ISM must be highly pressurized and must serve to prevent this dynamical expansion of individual components. Any substantial volume not filled by the H II gas must therefore be filled with hot (perhaps $10^6 - 10^7$ K), low density ($\sim 1 \text{ cm}^{-3}$), supernova-shocked plasma of the same pressure,

5.2. The Global Picture of the ISM in the Central 400 Parsecs.

The PDR models indicate that the incident FUV flux, G_0 , on each cloud is about the same as the average interstellar flux, G_{AV} , in the region contained in the beam (G_0 is derived from the PDR fine structure lines, whereas G_{AV} is derived from the beam-averaged radiation field seen in the FIR, see Appendix 11). This suggests that the OB stars might be randomly distributed throughout the volume of the emitting region, i.e., the stars are not spatially correlated with the clouds in the emission regions. Depending on whether the emission region is the disk, cylinder, or double hot spot described above, the average distance between the clouds is in the range 1.5-3.8 pc and the volume filling factors are $\phi_v \sim 8 \times 10^{-3}$ (disk), 1.6×10^{-2} (cylinder), and 0.11 (hot spots). Similarly, assuming 6×10^4 massive O stars provide the ionizing photons, the average distance between these stars is 7.6 pc (disk), 6.0 pc (cylinder) and 3.1 pc (hot spots). Since star-star gravitational interactions, cloud-cloud collisions, and star-cloud interactions will certainly induce relative motions of $> 31,111 \text{ s}^{-1}$ between a cloud and a massive star born in that cloud, we expect massive O stars to travel at least 10 pc from their natal cloud in their $\sim 3 \times 10^6$ year lifetime.

Therefore, it is not surprising that the stars are “randomized” with respect to the Clouds .

We propose a model in which randomly spaced O stars illuminate the compressed clumps of molecular gas between them. The pressure of the ISM is determined by frequent, supernovae blast waves, which maintain a hot $\sim 10^6$ K, pervasive intercloud medium (such as discussed in McKee & Ostriker 1977). The rate of supernovae explosions in the central 400 pc is taken to be $R_{SN} \sim 0.1 \text{ yr}^{-1}$ (see §1). The “porosity factor” Q (McKee 1992), which measures the volume filling factor of the hot intercloud medium, can be estimated from

$$Q \sim 0.7 \left(\frac{200 \text{ pc}}{R} \right)^3 n_I^{-0.11} \left(\frac{3 \times 10^6 \text{ cm}^{-3} \text{ K}}{\hat{P}} \right)^{1.36} \left(\frac{R_{SN}}{0.1 \text{ yr}^{-1}} \right), \quad (5.1)$$

where R is the radius of the entire region and n_I is the density in the hot intercloud plasma in cm^{-3} (we envision $n_I \sim 1 \text{ cm}^{-3}$ and temperature $T_I \sim 1 - 3 \times 10^6$ K, so that the pressure is the same as P_{PDR} and $P_{III} \sim 3 - 4 \times 10^6 \text{ cm}^{-3} \text{ K}$). $Q > 1$ indicates that the hot gas has a large volume filling factor (~ 1) and may drive a galactic superwind. If $Q \lesssim 1$, the pressure produced by the supernovae can be written $P = 2/3 S E t_{cool}$ (McKee & Ostriker 1977), where S is the supernova rate per unit volume, E is the kinetic energy in a typical supernova, and t_{cool} is the cooling time of the hot plasma. Using the cooling rate for $10^5 - 10^7$ K plasma from Cowie, McKee, & Ostriker (1981), we obtain for the pressure of the hot plasma

$$\hat{P} \sim 5 \times 10^6 E_{51}^{1/2} T_6^{1.3} \left(\frac{200 \text{ pc}}{R} \right)^{3/2} \left(\frac{R_{SN}}{0.1 \text{ yr}^{-1}} \right)^{1/2} \text{ cm}^{-3} \text{ K}, \quad (4)$$

where E_{51} is the supernova energy in units of 10^{51} ergs and $T_6 = T_I / 10^6$ K. Therefore,

assuming $E_{51} = 0.25$, $R = 200$ pc, $R_{SN} = 0.2 \text{ yr}^{-1}$, and $T_6 \sim 1$, we obtain $\hat{P} \sim 3 \times 10^6 \text{ cm}^{-3} \text{ K}$ and $Q \simeq 1$.

The solution is nicely self consistent. The supernovae would be expected to evaporate clouds until the density in the hot plasma is sufficient to allow most of the energy to be radiated away. This corresponds to $Q \sim 1$. At the same time, the volume filling factor of the hot plasma is high, of order unity. The pressure produced by the supernovae is exactly what is observed in the denser H II and PDR phases of the ISM if the hot plasma has a temperature $T \sim 1 \times 10^6 \text{ K}$. This temperature is typical for the interior of evolved SNR in clumpy ISM (see, for example, McKee 1992). The resultant pressure prevents the H II and PDR gas from expanding in a dynamical time of $\lesssim 3 \times 10^5 \text{ yr}$. Some of the hot plasma may escape from the central regions, producing the observed superwind in M82 (Chevalier & Clegg 1985). This model shows how a highly pressurized ISM is maintained, and predicts the value of the observed pressure.

6. SUMMARY AND CONCLUSIONS

As pointed out by, for example, Sofue (1987) and Yun et al. (1993), M82 experienced a severe gravitational encounter with M81 only 200 Myr ago, which initiated the formation of a bar. Regions where the leading dust lane crossed the outer-ILR bar are preferential sites for intense gas concentration and star formation (Kenney et al. 1993) because of the streamline crowding there and the subsequent frequent cloud-cloud collisions. The observed [O I] and [Si II] emission will naturally

originate in PDRs and 11 H regions in this vicinity, characterized by high gas density and ultraviolet fluxes and ongoing massive star formation.

We have argued for a PDR origin for the observed $[O\ I]\ 63\ \mu\text{m}$ emission and an H II region origin for most of the $[\text{Si}\ \text{II}]\ 35\ \mu\text{m}$ emission. Although the elemental abundance of silicon in the central 400 pc of M82 is probably about solar, the gas phase abundance of silicon is high, $\sim 1.5 \times 10^{-5}$, indicating that, only about half the silicon is incorporated in silicate grains. We speculate that a significant fraction of grains in this violent central region may have been vaporized by supernova shocks.

The PDR modeling of the neutral clouds in the central 400 pc of M82 indicates that they are numerous ($N_{cl} \sim 5 \times 10^3$), small ($r_{cl} \sim 0.4\text{--}1.0$ pc), dense ($n_a \sim 10^4\text{ cm}^{-3}$), and massive ($M_{cl} \sim 200\text{--}3000\ M_{\odot}$, although we note they are less massive than GMCs). We emphasize that the “clouds” may be clustered in sheets or filaments, so that r_{cl} represents the scale size (thickness or diameter) of the spherical, filamentary, or sheetlike clouds. In fact, we argue from the line profiles that the clouds are clustered in two hot spots, of size $125\text{ pc} \times 125\text{ pc}$, on either side of the center of the galaxy. Their volume filling factor in these hot spot regions is $\sim 10^{-1}$. The derived cloud properties in M82 are quite similar to those derived for NGC 253 by Carral et al (1994). Carral et al. found $N_{cl} \sim 2 \times 10^4$, $r_{cl} \sim 0.75\text{ pc}$, $n_a \sim 10^4\text{ cm}^{-3}$, and $M_{cl} \sim 2 \times 10^4\ M_{\odot}$ in NGC 253 with incident FUV fluxes perhaps 5–10 times that of M82.

The M82 clouds are highly pressurized. Their surfaces are illuminated by FUV

fluxes 103---104 times the average local (Milky Way) interstellar FUV flux. These high FUV fluxes represent the average FUV flux in the central 400 pc of M82. The FUV heats the atomic surfaces to ~ 250 K, resulting in pressures $P/k \sim 3 \times 10^6 \text{ cm}^{-3}$ K. With no external confining pressure, such clouds would expand and disappear in $\lesssim 3 \times 10^5$ years. However, the ionized gas in the central 400 pc of M82 fills a significant fraction, $\gtrsim 0.1$, of the ISM volume with gas of similar pressure ($n_e \sim 200 \text{ cm}^{-3}$ and $T \sim 10^4$ K). In addition, the frequent supernova shocks likely maintain the rest of the ISM at $T \sim 10^6$ K and $n_e \sim 1 \text{ cm}^{-3}$, thereby filling any remaining volume with plasma of equal pressure. The rate of supernova explosions determines the pressure in the ISM, compressing and pressurizing the H II regions and the neutral clouds. Pressure-confined, the clouds cannot expand freely. The large pressures in the entire central 400 pc of M82, three orders of magnitude higher than the average thermal pressure in our local ISM, maintain high densities in the cores of these clouds. Such pervasive high densities may lead to rapid star formation.

It appears that the interaction of M82 with M 81 created a central bar (Whit.11), in turn, induced the subsequent concentration of gas and dust in the central 400 pc of M82. The resulting high gas densities have caused a rapid rate of star formation. The large input of supernova shock energy has created a *hot* phase sufficiently pressurized to drive a strong superwind in M82. This pressure has also compressed the neutral clouds and may have accelerated the star formation rate. However, the fragmentation, photoionization, and photodissociation caused by the massive stars

is having a devastating effect on the molecular gas out of which these stars must presumably form. Already the clouds are sufficiently small or thin, and the UV flux sufficiently intense, that a significant fraction (~ 0.1) of the gas is photodissociated and warm (~ 250 K). Clearly the starburst will soon self-destruct, having destroyed the very environment necessary for its existence.

We are especially grateful to P. Duffy for motivating the original observations, and his work on the instrument, the observations and the $[0\ 1]$ data analysis. J. Wolf was of considerable assistance with both the instrument and the observations. We thank J. Baltz, P. Carral, and J. Simpson for their help during the flight series and to the staff of the Kuiper Airborne Observatory for their skillful support. C. McKee provided useful discussions. This work was supported by NASA under the RTOPs 188-44-53 and 352-02-03.

APPENDIX A.

DATA REDUCTION AND VELOCITY CALIBRATION

The [O I] and [Si II] observations were made in February 1986 and February 1987, respectively, and the [O I] line was reobserved in December 1990. The lines were observed using the facility Cryogenic Grating Spectrometer (CGS, Erickson et al. 1984; 1985; 1995) on the 91 cm telescope of the KAO. The instrumental beam was centered on the $2.2\ \mu\text{m}$ nuclear peak located at (1950 coordinates) $\alpha = 9^{\text{h}} 51^{\text{m}} 43^{\text{s}}.5$, $\delta = -69^{\circ} 55' 01''$ (Dietz et al. 1986) and had a FWHM of $34''$ and $44''$ for [Si II] and $44''$ for the 1987 [O I] observation (Table 3). The M82 [O I] spectra from 1990 and 1986 agreed well in width and shape, and the 1990 spectrum, while of lower signal-to-noise and more coarsely sampled, was useful in fixing the wavelength scale of the 1986 data. The 1990 data were taken with a $31''$ aperture and a $73\ \text{km s}^{-1}$ detector spacing. Offset guiding on nearby bright stars and boresight uncertainties yielded an rms pointing error of $\lesssim 5''$ during each observation.

Six Ge:Ga detectors were used for the first (1986) [O I] observation, and 13 Ge:Sb detectors were used for the second (1990) [O I] observations. For the [Si II] observation, 13 Ge:Be detectors were used. In each case, the full line width from M82's central region ($\Delta v \sim 400\ \text{km s}^{-1}$) is sufficiently large to require the use of multiple echelle grating settings for coverage of the entire line and nearby continuum.

The multiple observations overlapped in wavelength, oversampling the spectra by a factor of about 2. The velocity resolution for each observation is given in Table 3. The data were acquired while chopping with a 4' throw, oriented along the galaxy's minor axis. Sequences of four 10 s integrations were taken, with the source placed alternately in the left and right beam. The total integration time for each line was about one hour.

The galaxy spectra were corrected for the responsivity differences among detectors by dividing raw spectra of M82 by a spectrum of the KL nebula in Orion taken earlier in the flight at a nearby wavelength. An additional correction for the differences in detector responsivities and filter and grating efficiencies at the slightly differing wavelengths used on the KL nebula and M 82 was removed using spectra of a laboratory blackbody. These later corrections varied smoothly across the passband and were $\lesssim 15\%$ for the [O I] line and $\lesssim 30\%$ for the [Si II] line; they are known to $\lesssim 5\%$.

The [Si II] band is clear of atmospheric features, with 99% atmospheric transmission at the flight altitude of 41,000 feet. However, the [O I] line is strongly affected by a heavily saturated H₂O line located to the red of the [O I] line center. Even from the highest aircraft altitudes used on the 1986 flight (45,000 ft), the atmospheric transmission declines rapidly from $\sim 95\%$ at the shortest wavelength in our spectrum to $\leq 10\%$ at the longest, with a strong dependence on the overhead H₂O burden. Figure 1 shows our [O I] spectrum before correction for atmospheric absorption, as

well as several possible transmission curves.

Three criteria were used in determining the water column depths necessary to correct for atmospheric absorption. First, we determined a column depth of $\sim 8 \mu\text{m}$ of precipitable water towards KL at a flight altitude of 39,000 feet by measuring the spectrum of a telluric water line in absorption against the continuum emission of the nebula. We used this value to scale the output of the KA O aft zenith radiometer (also correcting for source elevation). At 43,000 feet, the scaled radiometer output indicated a rapidly varying column depth for the M82 observation 1 between 0 and $6 \mu\text{m}$ and at 45,000 feet it indicated about $1 \mu\text{m}$ of H_2O . Secondly, $1 \mu\text{m}$ more water was required at 43,000 feet than at 45,000 feet in order that the corrected flux densities taken at different altitudes be similar. Finally, we determined the water column such that the final continuum flux densities on the long wavelength side of the line were equal to those on the short wavelength side, where the absorption correction is small. All three criteria were met by $\lesssim 3 \mu\text{m}$ at 43,000 feet and $\lesssim 2 \mu\text{m}$ of water at 45,000 feet.

111 Figure 1 the data sets at two different altitudes have been renormalized to have the same continuum flux on the blue-shifted side of the line, and the atmospheric curves have been normalized to pass through this continuum, to allow a comparison of the continuum absorption on the red-shifted side of the line. The relatively small H_2O burden implies extremely dry stratospheric conditions, optimal for this observation.

Absolute flux calibrations were obtained by multiplying the ratioed spectra by the appropriate flux of KL at $35 \mu\text{m}$ and $63 \mu\text{m}$. The continuum fluxes for

KL were obtained from Erickson et al. (1981) and corrected for aperture differences using a 26" FWHM Gaussian model source distribution for K_L, as deduced from unpublished work of Werner (personal communication) and by our own observations in several different apertures. For the 1986 [O I] observations, and the 1987 [Si II] observations, calibration spectra of KL taken on two separate nights agreed to about 10%. Uncertainties in the KL and M82 source-line coupling models raise the total flux uncertainty to about 20% for each line, and cause a total error of about 15% for line ratios. Line ratios have a lower error because the lines share a common source distribution and model calibrator spectrum.

Absolute wavelengths were determined in a two step process. Firstly, V_{LSR} Doppler corrections and known instrumental offsets were removed from the data. Secondly, observations of [O I] in standard astronomical sources were used to eliminate errors in laboratory-determined wavelength calibration. The [Si II] observations were calibrated in this manner and yielded absolute wavelengths accurate to 20 km s⁻¹. The [O I] line velocity was calibrated using the 1990 source line profile and wavelength calibrators (Orion KL, IC 418, NGC 40) from the 1990 observations. Accurate wavelength determination for the [O I] line was also achieved within 20 km s⁻¹.

APPENDIX B

PDR MODELING OF ENSEMBLES OF CLOUDS IN GALACTIC NUCLEI

In the WTH model of the nucleus of a galaxy, N_{cl} identical, neutral, spherical clouds are present in the beam, each with a radius r_{cl} and an incident, external FUV flux given by G_0 , in units of $1.6 \times 10^{-3} \text{ ergs cm}^{-2} \text{ s}^{-1}$ (Habing 1968). These clouds emit [C II] $158 \mu\text{m}$, [O I] $63 \mu\text{m}$, $145 \mu\text{m}$, and [Si II] $35 \mu\text{m}$ line emission, as well as IR grain continuum from the warm, atomic, FUV illuminated outer layers (characterized by an average gas temperature T_a and a hydrogen nucleus density n_a). They also emit $^{12}\text{CO J=1} \rightarrow 0$ from cooler layers somewhat deeper into the clouds, as C^+ undergoes a transition to CO in the FUV-shielded regions. The area filling factor of these clouds is

$$\phi_a = \frac{N_{cl} \pi r_{cl}^2}{A_B}, \quad (B1)$$

where $A_B = \Omega D^2$ is the projected area of the beam (solid angle $= \Omega$) at the distance D of the galaxy. The total warm atomic mass in the beam is M_a .

The PDR models estimate n_a , G_0 , and ϕ_a from observations of [C II] $158 \mu\text{m}$, [O I] $63 \mu\text{m}$ and the IR grain continuum (see TH, HTH, and WHT). Given n_a , T_a , and the [C II] $158 \mu\text{m}$ luminosity (*i.e.*, knowing the distance to the galaxy) and assuming a gas phase C/H elemental abundance ratio, the model gives M_a .

To proceed to the final step of determining r_{cl} and N_{cl} , further assumptions are necessary. We assume that the molecular gas exists in identical spherical cores of these clouds, and that the ratio of the molecular hydrogen density of the core to the atomic surface density is given by

$$\eta = n_m/n_a. \quad (B2)$$

Note that the assumption of molecular cores is equivalent to assuming that $\Lambda_v \gtrsim 10$ through the clouds in regions with high FUV fluxes (TH). Using Equations (III) and (B2), we obtain

$$N_{cl} = \frac{16}{9} \frac{m_H^2 n_a^2 \phi_a^3 \Omega^3 D^6}{\pi (M_a + M_m / (2\eta))^2}, \quad (B3)$$

$$r_{cl} = \frac{3}{4} \frac{(M_a + M_m / (2\eta))}{m_H n_a \phi_a \Omega D^2}, \quad (B4)$$

where m_H is the mass of the hydrogen atom. With the exception of η , all parameters on the right hand side of the equations are constants or have been derived from observations. Molecular (e.g., CO J=1-0) or dust observations provide M_m ; such determinations of M_m have large error bars because of uncertainties in dust opacities in the FIR and in the conversion of molecular line luminosities to H_2 masses in galactic nuclei. Note that if $M_m / (2\eta) > M_a$, the effect of errors in M_m and/or η is large, especially in deriving N_{cl} , which is sensitive to the values of these as well as the physical parameters n_a , M_a , ϕ_a , and D . Insight into Equations (B3) and (B4) can be gained by noting that if the masses and densities are held fixed, it is the area filling factor which determines N_{cl} and r_{cl} : greater area filling factor requires more numerous small clouds. Less obvious in the equations is the fact that it is the ratio

of atomic mass to molecular mass which helps to fix N_{cl} and r_{cl} : since the atomic mass is proportional to the surface area of the clouds and the molecular mass is proportional to the volume, this ratio increases with increasing numbers of smaller clouds when the total mass is kept fixed.

If the clouds are in thermal pressure balance, η is about T_a/T_m , the ratio of the surface temperature to the temperature in the molecular core. The high FUV fields in galactic nuclei ($G_o \gtrsim 10^3$, cf. Crawford et al. 1985) result in surface temperatures $T_a \sim 300$ K (TH, ITT), and, assuming $T_m \sim 30$ K, thermal balance would suggest $\eta \sim 10$. Gravitationally bound clouds could result in even higher values of η . However, observations of the Orion PDR, for example (Crawford et al. 1986, Boreiko, Betz & Zmuidzinas 1988), show the linewidths of the $[C II] 158 \mu m$, $[O I] 63 \mu m$, and $CO J=1 \rightarrow 0$ lines are superthermal and ~ 5 km s $^{-1}$. Thus, thermal pressures are negligible and turbulent pressures dominate in the outer regions, and possibly in the cores as well. In such cases, the gas density may be approximately constant ($\eta \approx 1$). In the limit of a high density contrast or low molecular mass, $M_m/(2\eta) \ll M_a$, the solution for r_{cl} and N_{cl} asymptotes to a minimum value for r_{cl} and a maximum value for N_{cl} as the molecular core shrinks to insignificant size.

The volume filling factor ϕ_v of the clouds, assuming a spherical volume $\frac{4}{3}\pi R_B^3$ sampled in the galaxy, is given by

$$\phi_v = \frac{3\pi^{\frac{1}{2}} (NT_a + M_m/(2\eta))}{4\pi R_B^3 \Omega^{\frac{3}{2}} D^3} \quad (B5)$$

If, as is the case in M82, most of the bolometric luminosity in the beam is

from grain IR continuum, then we can calculate an “average FUV flux” G_{AV} in the sampled volume of the galaxy,

$$G_{AV} = \frac{f_{IR}}{A_B} (1.6 \times 10^3 \text{ ergs cm}^{-2} \text{ s}^{-1}), \quad (B6)$$

where $f \approx 0.5$ is the fraction of the incident radiation which lies in the FUV band and the factor in parenthesis is the standard unit of flux. The derived G_0 can then be compared with G_{AV} . If G_0 is roughly equal to G_{AV} , it could indicate that the illuminated clouds are randomly distributed in our beam volume and there is no spatial correlation between the illuminating sources and the clouds. Alternatively, it could indicate a central FUV source, and the illuminated clouds are randomly distributed in the beam, or at least, lie near the outer edges of the beam. However, if $G_0 \gg G_{AV}$, then, for example, the illuminating stars are correlated with the clouds, or the stars and clouds find themselves in a relatively small portion of the beam (see WTH).

APPENDIX C

DETERMINING THE MOLECULAR MASS

The total molecular content of the central region of M82 has proven difficult to measure. Estimates of total molecular mass span two orders of magnitude from 1×10^7 (Loiseau et al. 1990) to $\sim 1 \times 10^9 M_{\odot}$ (e.g., Carlstrom 1988). One reason for this situation is that $^{12}\text{CO J}=1-0$ emission alone is not a reliable tracer of molecular mass in this region. This becomes apparent from the fact that the “standard conversion” for $^{12}\text{CO J}=1-0$ to M_{H_2} (e.g. Young & Scoville 1984), which assumes that $^{12}\text{CO J}=1-0$ is optically thick, gives a molecular gas mass equal to the dynamical (stars+gas) mass estimated from the rotation velocity ($M=10^9 M_{\odot}$ for $V_{\text{circ}}=125 \text{ km s}^{-1}$, $R=3.75 \text{ pc}$, and $I_{\text{CO}}=6900 \text{ Jy km s}^{-1}$, Carlstrom 1988). This is an unlikely proposition, since the central region is known to have a high density stellar population (Telesco et al. 1991, Rieke et al. 1980).

The standard conversion is derived from an empirical correlation observed in molecular clouds, and can be explained by a model in which the line width is given by the virial velocity and the $\text{CO J}=1-0$ is optically thick with $T_{\text{ex}} \sim 10 \text{ K}$ (e.g. Dickman, Snell, & Schloerb 1986). The standard conversion is inappropriate for M82 because the assumption that M82 molecular clouds resemble Milky Way molecular clouds ($T_{\text{ex}} \sim 10 \text{ K}$) is not met (as illustrated by Maloney & Black 1988). The physical conditions in the central region of M82 are extreme, with a

high frequency of supernovae, strong UV fluxes, and regions of high ($n > 10^5 \text{ cm}^{-3}$) molecular density and excitation temperature (40 K). The high molecular gas temperature and densities are inferred from observations of CS, HCN, and high J-level CO transitions (Carlstrom 1988). Several authors have argued that the bulk of the CO emission must be optically thin because the observed ratio of brightness temperatures $T_b[\text{CO}(J=2-1)]/T_b[\text{CO}(J=1-0)]$ is greater than one. This model is not robust, since optically thin CO would have difficulty surviving rapid photodissociation in such an environment. However, conversions using optically thin CO distributions were used to make (lower limit) molecular mass estimates for the central region (e.g. Loiseau et al. 1990).

Another disquieting feature of the $J=1-0$ and $J=2-1$ CO maps is that they show a somewhat different spatial distribution of gas than the distribution of dust observed in the $\lambda=850 \mu\text{m}$ map. There are three CO ($J=1-0$) maxima seen in the interferometer maps (Carlstrom 1988; Shen & Lo 1995) spanning $25''$ - $30''$, while the submillimeter maps (Jaffe et al. 1984, $400 \mu\text{m}$; and Smith et al. 1990, $450 \mu\text{m}$) show a single, more centered emission region. The recent $450 \mu\text{m}$ continuum map of Hughes, Gear and Robson (1995) shows two peaks, separated by $1.5''$ but situated symmetrically around the $2.2 \mu\text{m}$ center with the Northeastern peak located inside of the E2 peak seen by Shen and Lo.

Fortunately, the situation has been significantly clarified in recent work by Wild et al. (1992). Their multi-level study includes maps of the ^{12}CO $J=6-5$, $J=3-2$,

J=2-1, J=1-0, C¹⁸O and C¹⁷O J= 2-1, HCN J=3-2, H¹³CN J= 1-0 and HCO⁺ J=3-2 emission in the central region of M82. Strong evidence that the ¹²CO emission is generally optically thick in all transitions comes from the intensity ratio of ¹²CO J=2-1 to C¹⁸O J=2-1 emission, which is found to be 25 to 43 across the nucleus, whereas a ratio equal to the ¹⁶O/¹⁸O abundance ratio, 500, would be expected for optically thin emission.

Wild et al. (1992) used seven observed line ratios to constrain the total CO column density, the molecular volume density, and the gas kinetic temperature, to derive a more accurate total mass. The line ratios were modeled using a non-LTE radiative transfer code, including clumpiness and opacity dependent filling factors (Eckart et al. 1990). Their conclusions are that the molecular clouds have an average density n_m of about $1 \times 10^4 \text{ cm}^{-3}$ and a kinetic temperature of about 45 K, with as much as 10% of the molecular gas distributed in an even denser cloud component, with $n_m \gtrsim 3 \times 10^5 \text{ cm}^{-3}$. Their mass distribution and total mass ($M_m = 1.8 \times 10^8 M_\odot$) are in good agreement with the 450 μm total mass and emission distribution. The mass peaks about $5''$ to the southwest of the center, but it falls off in density over $30''$, falling off slowly to the northeast. The derived mass distribution is also very similar to the 40 μm distribution shown in Figure 4. The mass in the northeast and southwest regions are roughly equal, $\frac{1}{2} M_m = 9 \times 10^7 M_\odot$.

In retrospect, the mass derived from the "standard conversion" is an overestimate of the molecular mass based on the ¹²CO J=1-0 alone principally because the

clouds are hot, not because *they* are optically thin. Likewise the smaller cloud size (see §3), and higher kinetic temperature and density cause the ^{12}CO J=1-0 transition to display a relative depression between the two lobes as compared with the more optically thin isotopic transitions which, like the mass, is strongly peaked toward the center.

Table 1
M82 Mid- and Far-Infrared Line Observations

Line	HPBW	cont. (Jy)	τ^c	Line Flux ^a (10^{-11} erg cm $^{-2}$ s $^{-1}$)	Num. of Positions	Ref.
Br α (4.1 μ m)	30''		0.8	3.6	13	1
[Ne II] (13 μ m) ^b	30'' \times 20''	0	8	28 \pm 8	13	1
	\sim 5''			25	4	2
[S III] (19 μ m)	25''	68	0.6	9.5 \pm 3.1	1	3
[S III] (33 μ m)	25''	556	0.3	15.7 \pm 1.9	1	3
[Si II] (35 μ m)	34''	487	0.3	13.543.3	1	4
[O III] (52 μ m)	48''	1207	0.19	10.4 \pm 0.8	1	5
	30''			8.2 \pm 2.5	1	6
[N III] (57 μ m)	48''	1269	0.17	4.3 \pm 0.4	1	5
[O I] (G3 μ m)	44''	1254	0.15	15.243.7	1	4
	30''			18.3-5.4	1	6
	44''			19. \pm 6	1	7
[O III] (88 μ m)	48''	1689	0.11	9.0 \pm 0.5	1	5
	45''			11. \pm 6	3	6
[N II] (122 μ m)	45''		0.05	2.9(+0.9)(-0.6)	1	8
[O I] (146 μ m)	55''		0.04	0.84 \pm 0.24	1	6
[C II] (158 μ m)	55''		0.04	14 \pm 4.2	5 \times 5	6,9
[N II] (205 μ m)	45''		0.02	0.71 \pm 0.12	3	8
[C I] (609 μ m)	15''		0.00	0.007 \pm 0.002	5	10

^aLine fluxes are quoted for the central position. ^bWe have integrated the 13 profiles to obtain the central flux in a 30" \times 20" region, and the uncorrected flux is about half the value reported by Gillett et al. (1975). "All line fluxes have been corrected for extinction by the factor $\exp(\tau)$, where τ has been drawn from the following dust models, using $A_V = 25$ mag (Puxley 1991; MeLeod et al. 1993). For $\lambda < 18 \mu$ m we use the dust models of Draine & Lee (1984) and Adams et al. (1988) averaged; for 18 and 33 μ m, we use H1011C1 et al. (1984) and Herter et al. (1981); for 34-57 μ m we use the λ^{-1} emissivity law as per Duffy et al. (1987); and for $\lambda > 57 \mu$ m we use the emissivity law of $\lambda^{-1.5}$ as per the results of Klein et al. (1988). References: (1) Beck et al. (1978); (2) Achtermann & Lacy; (3) Houck et al. (1984); (4) This work; (5) Duffy et al. (1987); (6) Lugten et al. (1986); (7) Watson et al. (1984); (8) Pietuchowski et al. (1994); (9) Stacey et al. (1991); (10) Schilke et al. (1993).

Table 2

Other Observations of M 82's Central 1 Disk

Observation	Result	Reference
Far-Infrared Continuum	$L_{FIR} = 3 \times 10^{10} L_{\odot}$	1
CO(J = 1-0, J = 2-1)	$M(H_2) = 1 \times 10^8 M_{\odot}$	2
Multiple Millimeter Transitions	$M(H_2) = 1.8 \times 10^8 M_{\odot}$	3
111 Absorption	$M(1-1) = 1.2 \times 10^7 M_{\odot}$	4

References:

(1) Telesco & Harper (1980).

(2) Carlstrom (1988).

(3) Wild et al. (1992).

(4) Weliachew et al. (1984).

Table 3

[O I] and [Si II] Line Parameters

Line	[O I]	[Si II]	FWHM	Resolution	Continuum	Line Flux ^a	Intensity ^b	Luminosity
[O I] 63.184 μm	44"	106	km s ⁻¹	1254 \pm 26 ^c	Jy	13.1 \pm 0.2 ^c	13.4 \pm 0.2 ^d	5.4 $10^7 L_{\odot}$
[Si II] 34.814 μm	34"	81	km s ⁻¹	487 \pm 101 ^c	Jy	10.9 \pm 0.3 ^c	11.1 \pm 0.3 ^d	4.5 $10^7 L_{\odot}$
[Si II] 34.814 μm	44"	104	km s ⁻¹			12. ^e		4.9 $10^7 L_{\odot}$

^aLine Flux is in units of 10^{-11} erg cm⁻² s⁻¹ with no extinction corrections applied.^bIntensity is in units of 10^{-3} erg cm⁻² s⁻¹ sr⁻¹^cThese are statistical errors excluding systematic calibration errors.^dThese values are computed assuming the [O I] and [Si II] emission is uniform over a 30" x 14" area (9.8×10^{-9} steradians). In actuality, the emitting regions are probably smaller and these intensities are lower limits (see text).^eThe line flux error and continuum level were not measured, but are comparable to the 34" measurement.

Table 4
Gaussian Fit Results

Region	Parameter	[O I] 63 μm	[Si II] 35 μm	[C II] 158 μm ^a
Northeast	Line Flux (10^{11} erg cm ⁻² s ⁻¹)	5.9 \pm 0.7 ^b	4.4 \pm 1.3	4.3 \pm 0.9
	V_{LSR} (km s ⁻¹)	325 \pm 8	307 \pm 21	.
	FWHM (km s ⁻¹)	173 \pm 21	180 \pm 37	
Southwest	Line Flux	7.2 \pm 0.6	6.5 \pm 1.2	9.9 \pm 2.0
	V_{LSR}	148 \pm 5	130 \pm 11	
	FWHM	145 \pm 8	176 \pm 21	
Total	Line Flux	13.1 \pm 0.2	10.9 \pm 0.3	14.2 \pm 3.0
	N (data points)	42	36	19
	Reduced χ^2	2.3	3.0	1.4
	Continuum Flux (Jy)	1254 \pm 26	487 \pm 101	

^aUsing [C II] 158 μm line profile from Crawford et al. (1985)

^bThe error terms were obtained by fitting to many data sets, where the different sets were produced by varying individual data points according to their statistical uncertainties.

Table 5

PDR Parameters

Model	Area	Log (n)	Log (G_0)	$M_a(M_\odot)$	ϕ_a	$(\frac{O}{SiII})_{model}$	$(\frac{O}{SiII})_{obs.}$	(SiII) $\frac{obs.}{model}$	FIR
1	Total	3.9	3.0	3.2 x 10 ⁷	1.0	63	1.7	52	9.3×10 ⁻⁸
2	Northeast	3.9	3.4	9.6 x 10 ⁶	2.0	58	1.3	44	5.1×10 ⁻⁸
2	Southwest	3.9	2.9	2.0 x 10 ⁷	6.3	70	1.1	63	4.2×10 ⁻⁸
3	Northeast	3.9	3.4	9.6 x 10 ⁶	6.6	58	1.3	44	5.1×10 ⁻⁸
3	Southwest	3.9	2.9	2.0 x 10 ⁷	21	70	1.1	63	4.2×10 ⁻⁸

Cloud Parameters

Model	Region	Size (sr)	N_{cl}	r_{cl} (pc)	M_{cl}	M_a	M_m	M_{total}	T_a (K)	ϕ_v	r_m (pc)
1	Total	9.9 x 10 ⁻⁹	3.3×10 ⁵	0.6	545	3.2 x 10 ⁷	1.8 x 10 ⁷	1.8×10 ⁸	230	0.013	0.5
2	Northeast	4.9×10 ⁻⁹	3.3 x 10 ⁴	1.0	3030	9.6×10 ⁶	9.0×10 ⁷	1.0×10 ⁸	240	0.015	0.8
2	Southwest	4.9 x 10 ⁻⁹	5.0×10 ⁵	0.4	220	2.0×10 ⁷	9.0×10 ⁷	1.1×10 ⁸	220	0.021	0.3
3	Northeast	1.5×10 ⁻⁹	3.3 x 10 ⁴	1.0	3030	9.6×10 ⁶	9.0×10 ⁷	1.0×10 ⁸	240	0.09	0.8
3	Southwest	1.5×10 ⁻⁹	5.0 × 10 ⁵	0.4	220	2.0 × 10 ⁷	9.0×10 ⁷	1.1×10 ⁸	220	0.13	0.3

Notes: Global parameters for gas clouds in $\sim 45''$ beam assuming a $30 \times 14''$ disk (Model 1), two regions of half this size on either side of the nucleus (Model 2) and two “hot spots,” $8''$ in diameter (Model 3): n (cm^{-3}) is the density of the warm atomic gas; G_0 is the incident FUV flux in units of the average interstellar radiation field (ISRF); Masses are in units of M_\odot ; M_{cl} is the typical cloud mass; M_a is the total warm atomic gas mass; ϕ_a is the area filling factor of this component; FIR ($\text{erg cm}^{-2} \text{s}^{-1}$) is the far-infrared continuum flux as determined by Rieke et al. (1980) and separated into the two regions on the basis of the $40 \mu\text{m}$ results of Joy et al. (1987); M_m is the total molecular mass determined by Wild et al. 1992 and divided between the regions on the basis of Carlstrom (1988); T_a is the temperature of the warm atomic component; N_{cl} is the number of clouds; r_{cl} is the typical cloud radius; ϕ_v is the volume filling factor of neutral cloud material (molecular and atomic); and r_m (pc) is the radius of a typical molecular cloud core.

REFERENCES

- Achtermann, J. M. & Lacy, J. H. 1995, *ApJ*, **163**, 175
- Adams, F. C., Lada C. J., & Shu F. H. 1988 *ApJ*, **326**, 865
- Beck, S. C., Lacy, J. H., Baas, F., & Townes, C. H. 1978, *ApJ*, **226**, 545
- Borciko, R. T., Betz, A. L., & Zmuidzinas, J. 1988, *ApJ*, **325**, 147
- Burton, M. G., Hollenbach, D. J., & Tielens, A. G. G. M. 1990, *ApJ*, **365**, 620
- Carroll, P., Hollenbach, D., Lord, S., Colgan, S., Haas, M., Rubin, R., & Erickson, E. 1994, *ApJ*, **423**, 223
- Carlstrom, J. E. 1988, Ph. D. thesis, University of California, Berkeley
- Carlstrom, J. E. 1991 & Kronberg, P. P. 1991, *ApJ*, **366**, 422
- Chevalier, R. A. & Clegg, A. W. 1985, *Nature*, **317**, 44
- Combes F. & Gerin M. 1985, *A & A*, **150**, 327
- Cowie, L. L., McKee, C. F., & Ostriker, J. P. 1981, *ApJ*, **247**, 908
- Crawford, M. K., Genzel, R., Townes, C. H., & Watson, W. M. 1985, *ApJ*, **291**, 755
- Crawford, M. K., Lugten, J. B., Pitelson, W., Genzel, R. & Melnick, G. 1986, *ApJ*, **303**, L57
- Dickman, R. L., Snell, R. L. & Schloerb, F. P. 1986, *ApJ*, **303**, 326.
- Dietz, R. D., Smith, J., Hackwell, J. A., Gehr, R. D. & Grasdalen, G. L. 1986, *AJ*, **91**, 758
- Draine, B. T. & Lee, M. 1984, *ApJ*, **285**, 89
- Draine, B. T. & Woods, D. T. 1990, *ApJ*, **363**, 464
- Duffy, P. B., Erickson, E. F., Haas, M. R., & Houck, J. R. 1987, *ApJ*, **315**, 68
- Eckart, A., Downes, D., Genzel, R., Harris, A. L., Jaffe, D. T., & Wild, W. 1990, *ApJ*, **348**, 434
- Erickson, E. F., Kracke, R. F., Tokunaga, A. T., & Haas, M. R. 1981, *ApJ*, **245**, 148
- Erickson, E. F., Matthews, S., Augason, G. C., Houck, J. R., Rank, D. M., & Haas, M. R. 1984, *Proc. SPIE*, **509**, 129

- Erickson, E. F., Houck, J. R., Harwit, M., Rank, D. M., Haas, M. R., Hollenbach, D. J., Simpson, J. P., Augason, G. C., & McKibben, D. D. 1985, *Infrared Physics*, **25**, 513
- Erickson, E. F., Colgan, S. W. J., Simpson, J. P. & Rubin, R. H. 1995, *Airborne Astronomy Symp. on the Galactic Ecosystem: From Gas to Stars to Dust*, ASP Conf. Series, ed. M. R. Haas, J. A. Davidson, & E. F. Erickson, (San Francisco: ASP), p. 523
- Gillett, F. C., Kleinmann, D. E., Wright, F. L., & Capps, R. W. 1975, *ApJ*, **198**, L65.
- Graf, P. 1988, PhD thesis, Cornell University, Ithaca
- Graf, P., Herter, T., Gull, G. E., & Houck, J. R. 1988, *ApJ*, **330**, 803
- Güsten, R. and Mezger, P. G. 1983, *Vistas in Astronomy*, **26**, 159
- Haas, M. R., Hollenbach, D. J., & Erickson, E. F. 1986, *ApJ*, **301**, L57
- Heckathorn, H. M. 1972, *ApJ*, **173**, 501
- Heckman, T. M., Armus, L., & Miley, G. K. 1990, *ApJ Supp*, **74**, 833
- Herter, T., Helfer, H. J., Pipher, J. I., Forrest, W. J., McCarthy J., Houck, J. R., Willner, S. P., Puetter, R. C., Rudy, R. J., & Soifer, B. T. 1981, *ApJ*, **250**, 186
- Hollenbach, D. J. 1990, in *The Evolution of the Interstellar Medium*, ed. L. Blitz, (ASP Publishers: San Francisco), p167
- Hollenbach, D. J. & McKee, C. F. 1989, *ApJ*, **342**, 306
- Hollenbach, D. J., Takahashi, T., & Tielens, A. 1991, *ApJ*, **377**, 192 (HTT)
- Hollenbach, D. J. & Tielens, A. G. G. M. 1995, in *Proceedings of the Physics and Chemistry Of Interstellar Molecular Clouds*, Lecture Notes in Physics, ed. G. Winnewisser (Springer: Berlin), in press
- Houck, J. R., Shure, M. A., Gull, G. E., & Herter, T. 1984, *ApJ*, **287**, 1,11
- Hughes, D. H., Gear, W. K., & Robson, E. I. 1994, *MNRAS*, **270**, 641
- Jaffe, D. T., Becklin, E. E. & Hildebrand, R. H. 1984, *ApJ*, **285**, L31
- Joy, M., Lester, D. P., & Harvey, P. M. 1987, *ApJ*, **319**, 314
- Kenney, J. D. D., Wilson, C. D., Scoville, N. Z., Devereux, N. A., Young, J. S. 1992, *ApJ*, **395**, L79 1995 *ApJ*...441..549Q
- Kenney, J. 1995, in *The ISM in Galaxies*, IAU Conference Proceeding, ed. J. M. van der Hulst, Kluwer, in press
- Klein, U., Wielebinski, R. & Morsi, H. W. 1988, *A A*, **190**, 41

- Kronberg, P. P., Biermann, P., & Schwab, F. R. 1985, *ApJ*, 291, 693
- Larlin, J. E., Graham, J. R., Matthews, K., Soifer, B. T., Beckwith, S., Herbst, T. M., & Quillen, A. C. 1994, *ApJ* 420, 159
- LeVan, P. D. & Price, S. D. 1987, *ApJ* 312, 592
- Loiseau N., Nakai, N., Sofue, Y., Wielebinski, R., Reuter, H.-P., & Klein, U. 1990, *AA*, 228, 331
- Lugten, J. B., Watson, D. M., Crawford, M. J., & Genzel, R. 1986, *ApJ*, 311, L51
- Maloney, P. & Black, J. H. 1988, *ApJ*, 325, 389
- Maloney, P., Hollenbach, D. J., & Tielens, A. G. G. M. 1995, *ApJ*, in press
- Mauersberger, R. & Henkel, C. 1991, *AA*, 245, 457
- McKee, C. P. 1992, in *Evolution of the Interstellar Medium*, ed. L. Blitz (San Francisco:ASP), 3
- McKee, C. P., & Ostriker, J. P. 1977, *ApJ*, 218, 148
- McLeod, K. J., Rieke, G. H., Rieke, M. J. & Kelly, D. M. 1993, *ApJ* 412, 111
- Meixner, M., Haas, M. R., Tielens, A. G. G. M., Erickson, E. F., & Werner, M. 1992, *ApJ*, 390, 499
- Miller, G. E. & Scalo, J. M. 1979, *ApJ Suppl*, 41, 513
- IvJuxlow, J. W. B., Pedlar, A., Wilkinson, P. N., Axon, D. J., Sanders, E. M., & de Bruyn, A. G. 1994, *MNRAS*, 266, 455
- O'Connell, R. W. & Manganaro, J. J. 1978, *ApJ*, 221, 62
- Petuchowski, S. J., Bennett, C. L., Haas, M. R., Erickson, E. F., Lord, S. D., Rubin, R. H., Colgan, S. W. J. & Hollenbach, D. J. 1994, *ApJ*, 427, 1, 17
- Puxley, P. J. 1991, *MNRAS*, 249, 11p
- Rieke, G. H., Lebofsky, M. J., Thompson, R. L., Low, F. J., & Tokunaga, A. T. 1980, *ApJ*, 238, 24
- Rubin, R. H. 1985, *ApJ Supp*, 57, 349
- Rubin, R. H., Dufour, R. J., & Walter, D. K. 1993, *ApJ*, 413, 242
- Rubin, R. H., Simpson, J. P., Erickson, E. F., & Haas, M. R. 1988, *ApJ*, 327, 377
- Sequist, E. R., Bell, M. B. & Bignell, R. C. 1985, *ApJ*, 294, 546

- Shen, J. & Lo, K. Y. 1995, *ApJ*, 445, 1,99
- Schilke, P., Carlstrom, J. E., Keene, J., Phillips, T. G. 1993, *ApJ*, 417, 1,67
- Smith, J. A., Brand, P. W. J. L., Puxley, P. J., Mountain, C. M., Nakai, N. 1990, *MNRAS*, 243, 97
- Sofue, Y. 1988, in *Galactic and Extragalactic Star Formation*, ed. R. Pudritz & M. Fich, (Dordrecht: Kluwer), 409
- Stacey, G. J., Geis, N., Genzel, R., Lugten, J.B., Poglitsch, A., Sternberg, A., & Townes, C.H. 1991, *ApJ*, 373, 423
- Statler, G.J., Jaffe, D. T., Geis, N., Genzel, R., Harris, A. I., Poglitsch, A., Stutzki, J. & Townes, C. H. 1993, *ApJ*, 404, 219
- Sternberg, A. & Dalgarno, A. 1989. *ApJ*, 338, 197
- Tammann, G.A. & Sandage, A. 1968, *ApJ*, 151, 825
- Telesco, C. M., Campins, H., Joy, M., Dietz, R., & Decher, R. 1991, *ApJ*, 369, 135
- Telesco, C. M. & Gezari, D. Y. 1992, *ApJ*, 395, 461
- Telesco, C. M. & Harper, J. A. 1980, *ApJ*, 235, 392
- Tielens, A. G. G. M. & Hollenbach, D. 1985, *ApJ*, 291, 722 (T1)
- Tutukov, A. & Krugel, F. 1981 *Soviet Astr.*, 24, 539
- Ulvestad, J. S. & Antonucci, R. R. J. 1994, *ApJ*, 424, L29
- Van Buren, D. 1985, *ApJ*, 294, 567
- Van Buren, D. & Greenhouse, M. A. 1994, *ApJ*, 431, 640
- Van Steenberg, M.E. & Shull, J. M. 1988, *ApJ*, 330, 942
- Waller, W. H., Gurwell, M. and Tamura, M. 1992, *AJ*, 104, 63
- Watson, J. M., Genzel, R., Townes, C. H., Werner, M. W., & Storey, J. W. V. 1984, *ApJ*, 279, 1,1
- Weliachew, L., Pomalont, E.B., & Greisen, E. W. 1984, *A&A*, 137, 335
- Werner, M. W., Crawford, M. K., Genzel, R., Hollenbach, D. J., Townes, C. H., & Watson, J. M. 1984, *ApJ*, 282, L81
- Wild, W., Harris, A. I., Eckart, A., Genzel, R., Graf, U. U., Jackson, J., Russell, A. P. G., Stutzki, J. 1992, *A&A*, 265, 447

- Willner, S. P., Soifer, B. T., Russell, R. W., Joyce, R. R., & Gillett, F. C. 1977, *ApJ*, 217, L121
- Wolfire, M., Hollenbach, D. J. & Tielens, A. G. G. M. 1989 *ApJ*, 344 770
- Wolfire, M., Tielens, A. G. G. M. & Hollenbach D. J. 1990 *ApJ*, 358, 116 (WTH)
- Young, J. S. & Scoville, N. Z. 1984, *ApJ*, 287, 153
- Yun, M. S., Ho, P. T., & Lo, K. Y. 1995, *ApJ*, 411, 1,17

FIGURE CA. PTIONS

Figure 1: The $63.184 \mu\text{m } ^3P_1 \rightarrow ^3P_2$ transition of [O I] in M82 is shown before correction for absorption in the earth's atmosphere. Data taken at 41,000 feet are plotted with open circles and data taken at 45,000 feet are plotted with filled circles. The lower four curves represent models of the uncorrected continuum flux as seen at an altitude of 45,000 feet subject to atmospheric absorption. The curves from top to bottom correspond to 1, 3, 5, and 1011111 of precipitable water along the line of sight.

Figure 2: A comparison is made of the corrected [O I] $63 \mu\text{m}$ and [Si II] $35 \mu\text{m}$ profiles, showing the velocity peak at $\sim 145 \text{ km s}^{-1}$ and the shoulder at $\sim 320 \text{ km s}^{-1}$.

Figure 3: Observations of H II transitions are shown along with the predictions using the models of Rubin (198L), for a collection of $6 \times 10^4 \text{ H II}$ regions with electron density $n_e = 190 \text{ cm}^{-3}$. The Lyman continuum luminosity of the central star in each region is taken as 10^{49} s^{-1} , in order to match the total Lyman continuum output, determined from the thermal radio emission (Carlstrom 1988). The Br α and [Ne III] fluxes required large extinction corrections, as per Table 1. The observed [Si I II] and [C II] fluxes overshoot the predictions. This indicates that [CII] more likely originates in PDR regions outside the H II regions. However, the model [Si I II] flux is low because of the adopted gas phase silicon abundance in the H II region model (see text).

Figure 4: a) **Spatial distribution of the central emission in M82** (adapted from Telesco et al. 1991). In the left panel, top to bottom: the 6 cm map of Kronberg et al.(1985) showing discrete SNRs at $0''.34$ resolution; the CO(J=1-0) map of Shen and Lo (1995) at $2''.5$ resolution; and the H I opacity map of Weliachew et al. (1984) at $3''.8 \times 6''$ resolution. In the right panel, from top to bottom: a schematic adapted from Mauersberger & Henkel (1991) showing the CS and other tracers of dense molecular gas found in extended hot spots; the $30 \mu\text{m}$ distribution of Telesco et al. (1991) at $5''$ resolution; and the $40 \mu\text{m}$ continuum emission in solid contours from Joy et al. (1987) from their Table 2 and Figure 9. The dashed lines are the I ICY isovelocity contours of Heckathorn (1972) running 135 km s^{-1} in the southwest to 315 km s^{-1} in the northeast by increments of 30 km s^{-1} . The solid circle shows the $44''$ beam used to make the [O I] observations. The filled circles are the inferred location of the hot spots producing the [O I] and [Si II] emission (see text).

Figure 5: The [O I] and [Si II] fluxes observed in two different apertures, plotted against aperture size, A . The dotted line is a model where $\text{Flux} \sim A^2$, which corresponds to an extended uniform distribution. The dashed line corresponds to flux distributed like the $26'' \times 13''$ $40 \mu\text{m}$ distribution seen by Joy et al. (1987). The observations are more consistent with the $40 \mu\text{m}$ flux distribution.

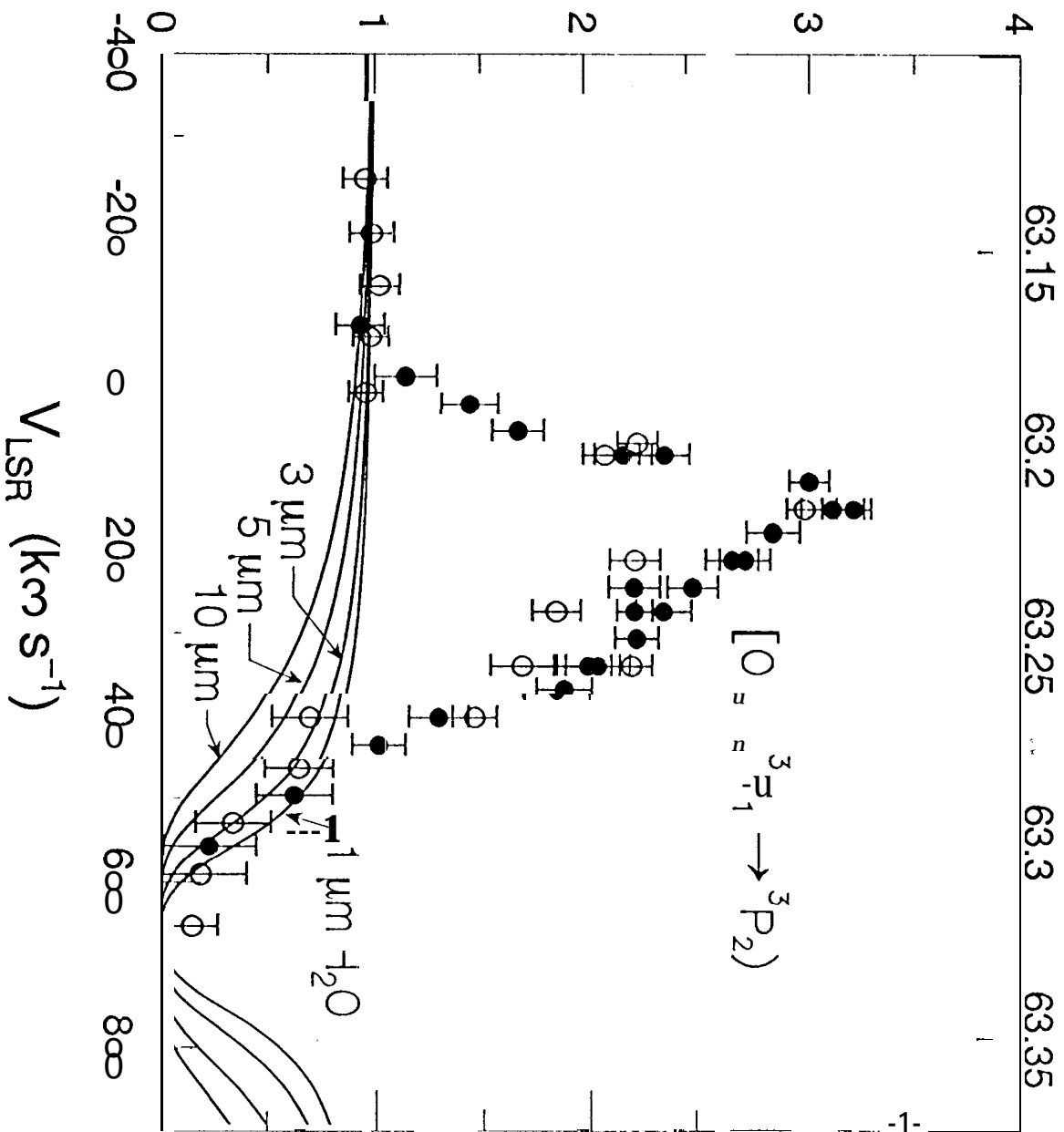
Figure 6: (a) The observed [O I] $63 \mu\text{m}$ and (b) [Si II] $35 \mu\text{m}$ data with a two component Gaussian fit (using six free parameters).

Figure 7: The observed emission distributions (left column) and the resulting synthetic

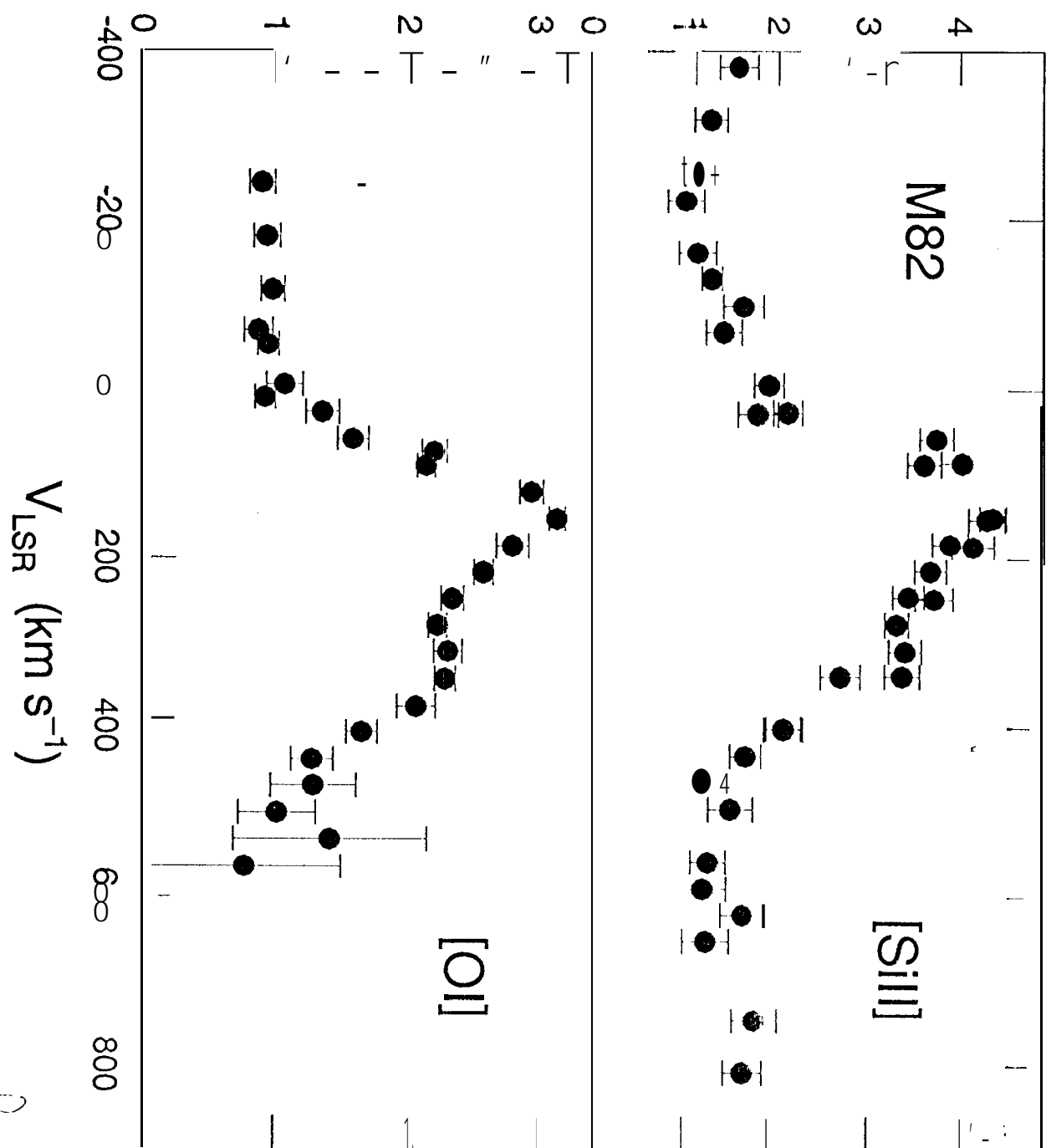
line profiles (right, column). The emission distributions are: (a) the $12.4\ \mu\text{m}$ distribution (Telesco & Gezari 1992); (b) the $40\ \mu\text{m}$ distribution (Joy et al. 1987); the $3.3\ \text{mm}$ continuum (Carlstrom & Kronberg 1991); (c) the CO emission (Shen & Lo 1995); and two versions of the bilobal model for the [O I] and [Si II] emission presented in the text: (i) $8''$ hot spots; and (k) $2''$ hot spots. All panels (j) and (k.) we also show the observed [O I] line profile with a dashed line for comparison. To produce the synthetic line profiles, we have used the $\text{H}\alpha$ velocity field of (Heckathorn 1972) and the velocity dispersion at each location measured from major axis CO measurements (Carlstrom 1988). The resulting “line profiles” in b,d,f, and h all resemble a single peaked Gaussian, and are dissimilar to the observed [O I] and [Si II] profiles. The dual hot-spot model replicates the observed fine `strut.tmc` profiles with the pronounced $320\ \text{km s}^{-1}$ shoulder seen in observed spectra in panels j and l.

Wavelength (μm)

Flux Density (10^{-9} ergs $\text{cm}^{-2}\mu\text{m}^{-1}$)



Flux Density (10^{-9} ergs $\text{cm}^{-2}\text{pm}^{-1}$)



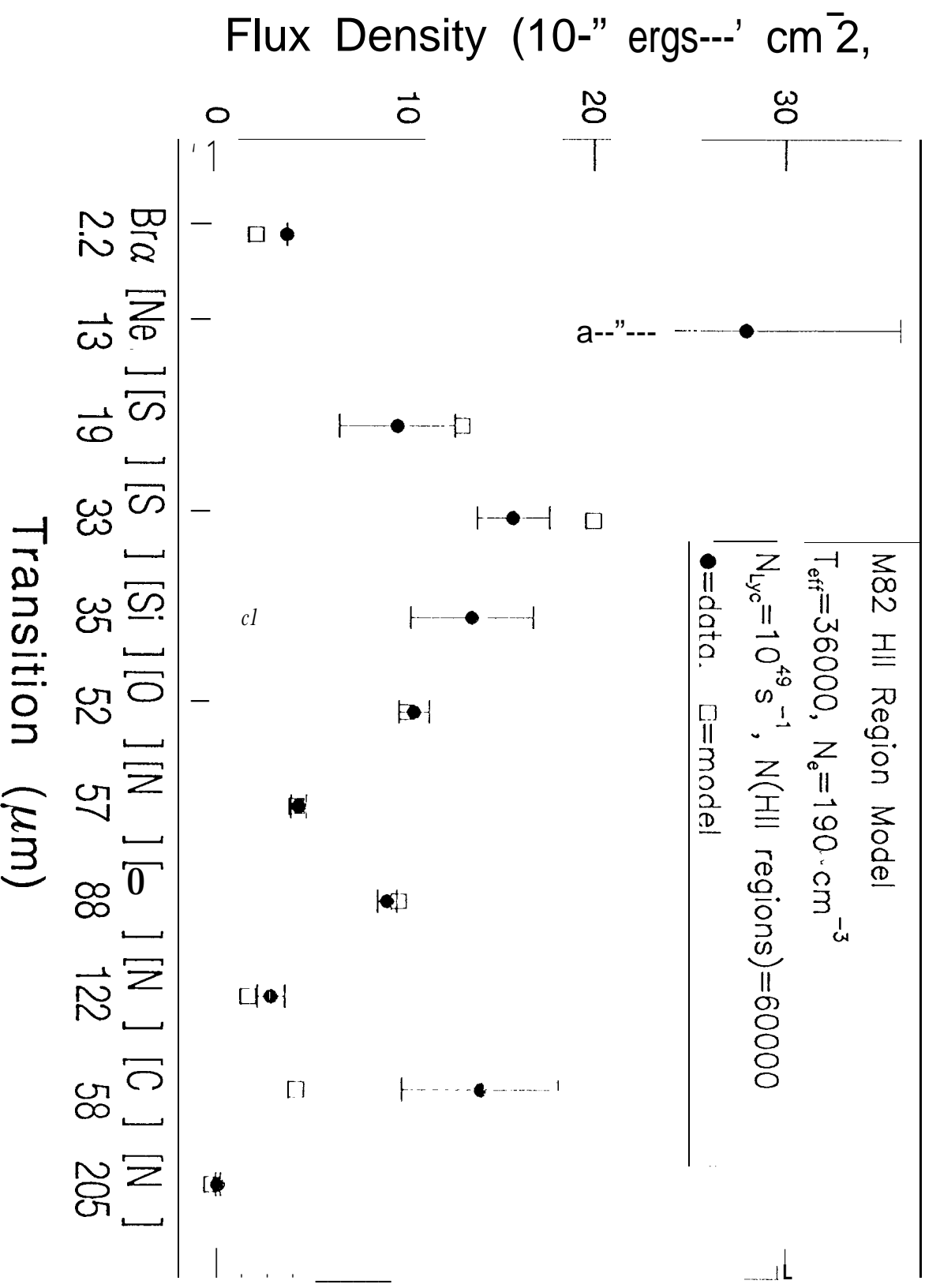
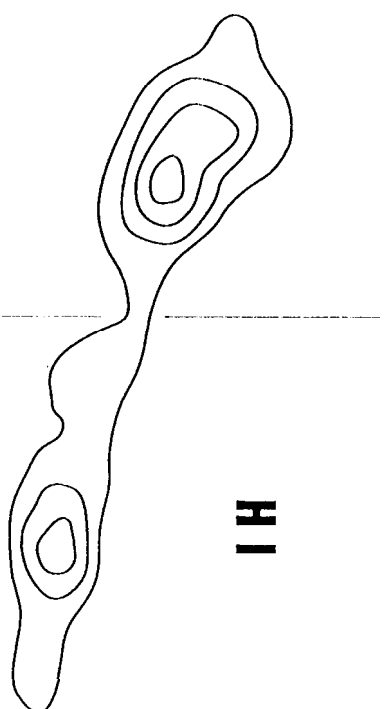
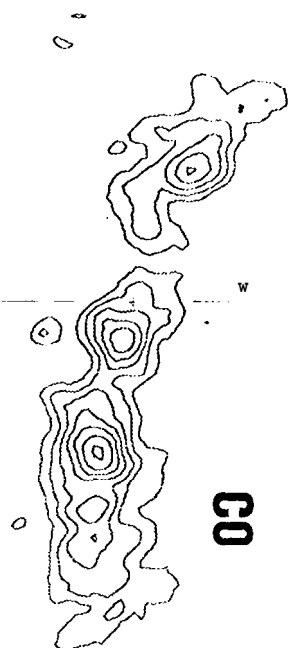
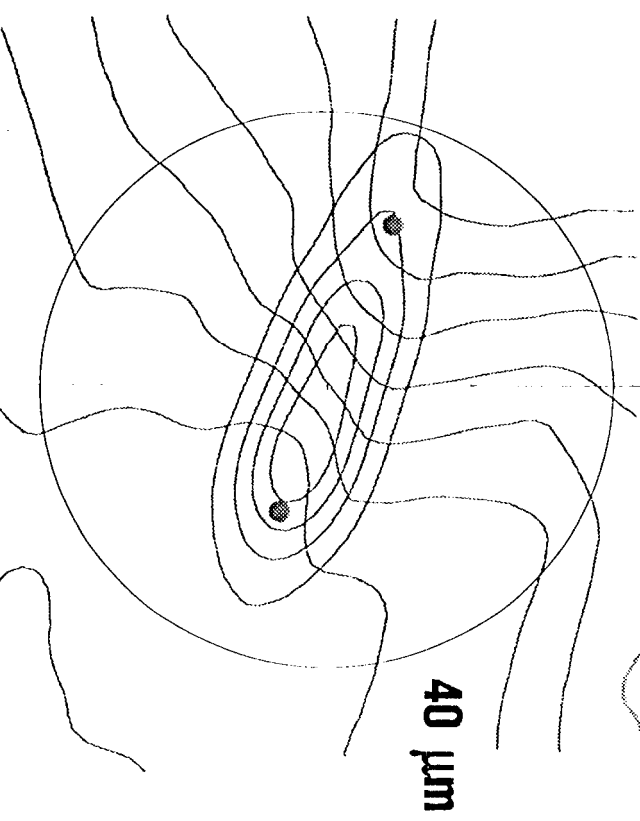
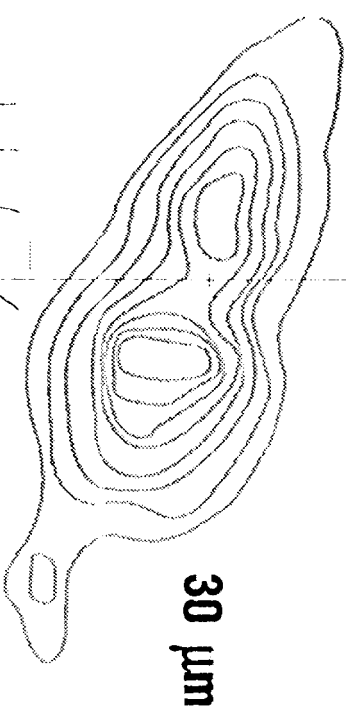
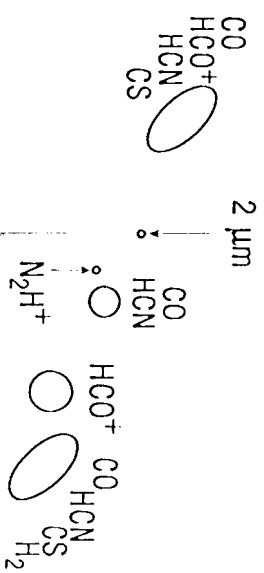


Fig 3



20 _____ 0 _____ -20
R.A. offset (")



20 _____ 0 _____ -20
R.A. offset (")

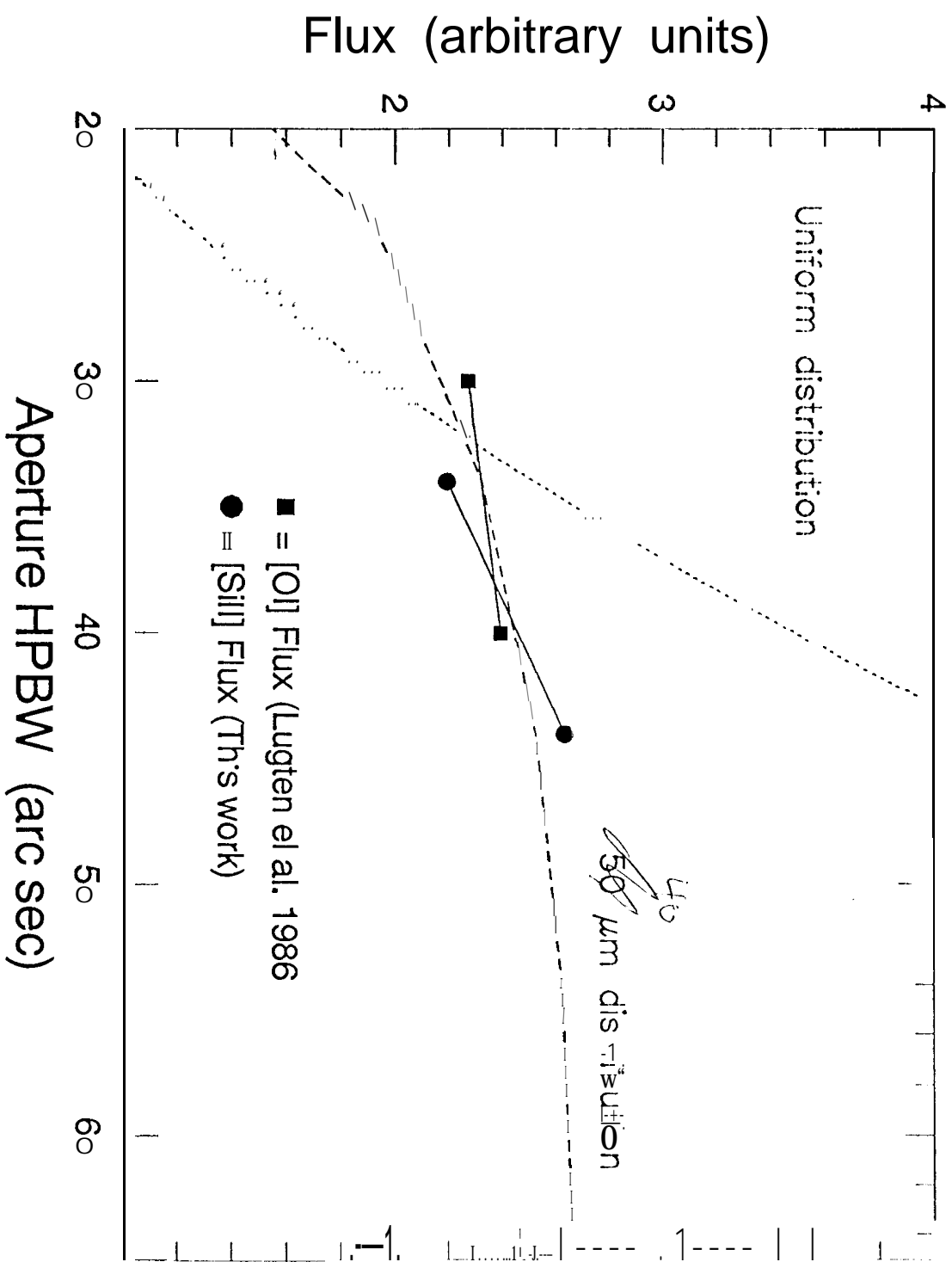


fig 5

Flux Density (10^{-9} ergs $\text{cm}^{-2}\text{pm}^{-1}$)

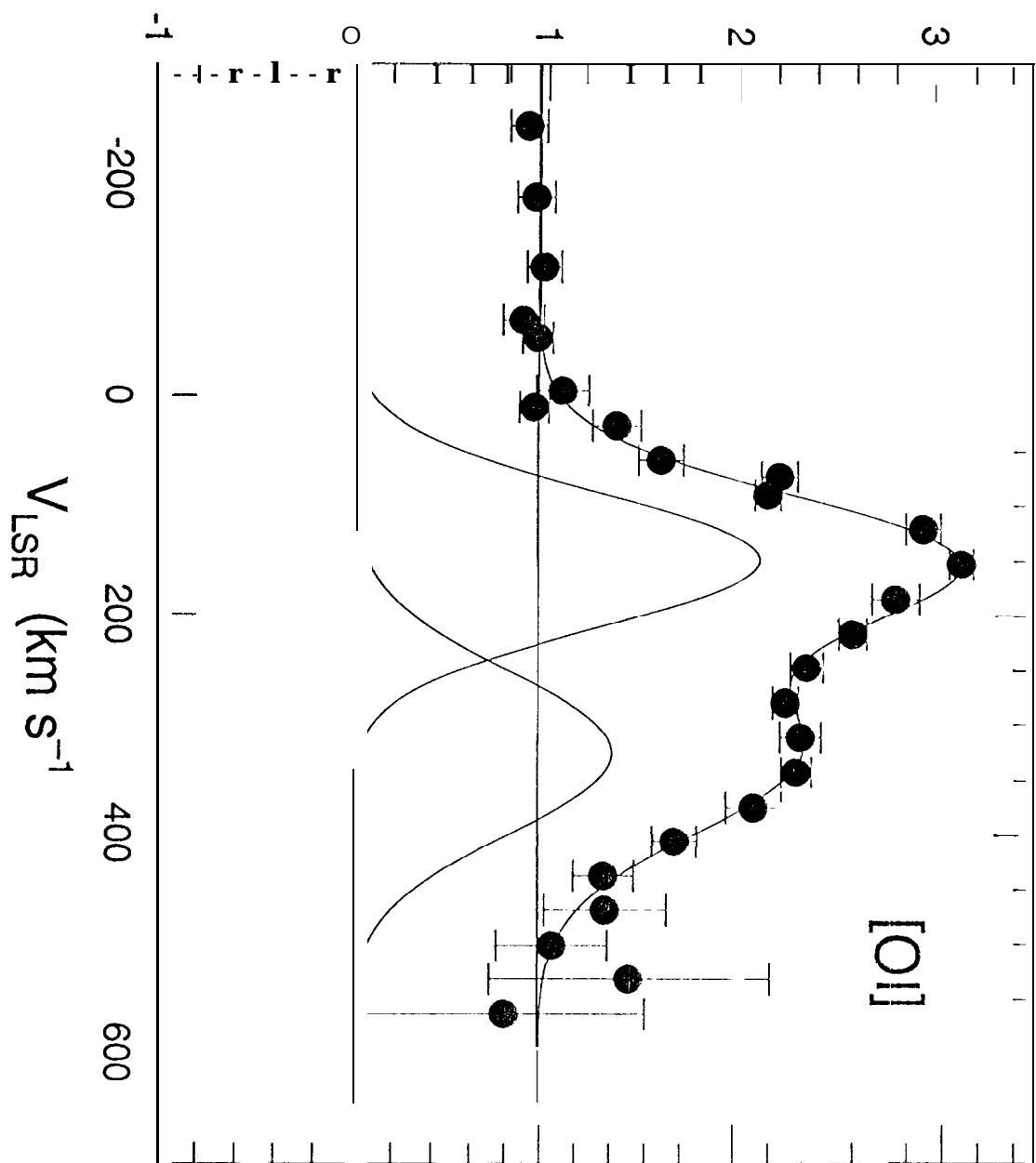


Fig 6a

Flux Density (10^{-9} ergs $\text{cm}^{-2}\text{pm}^{-1}$)

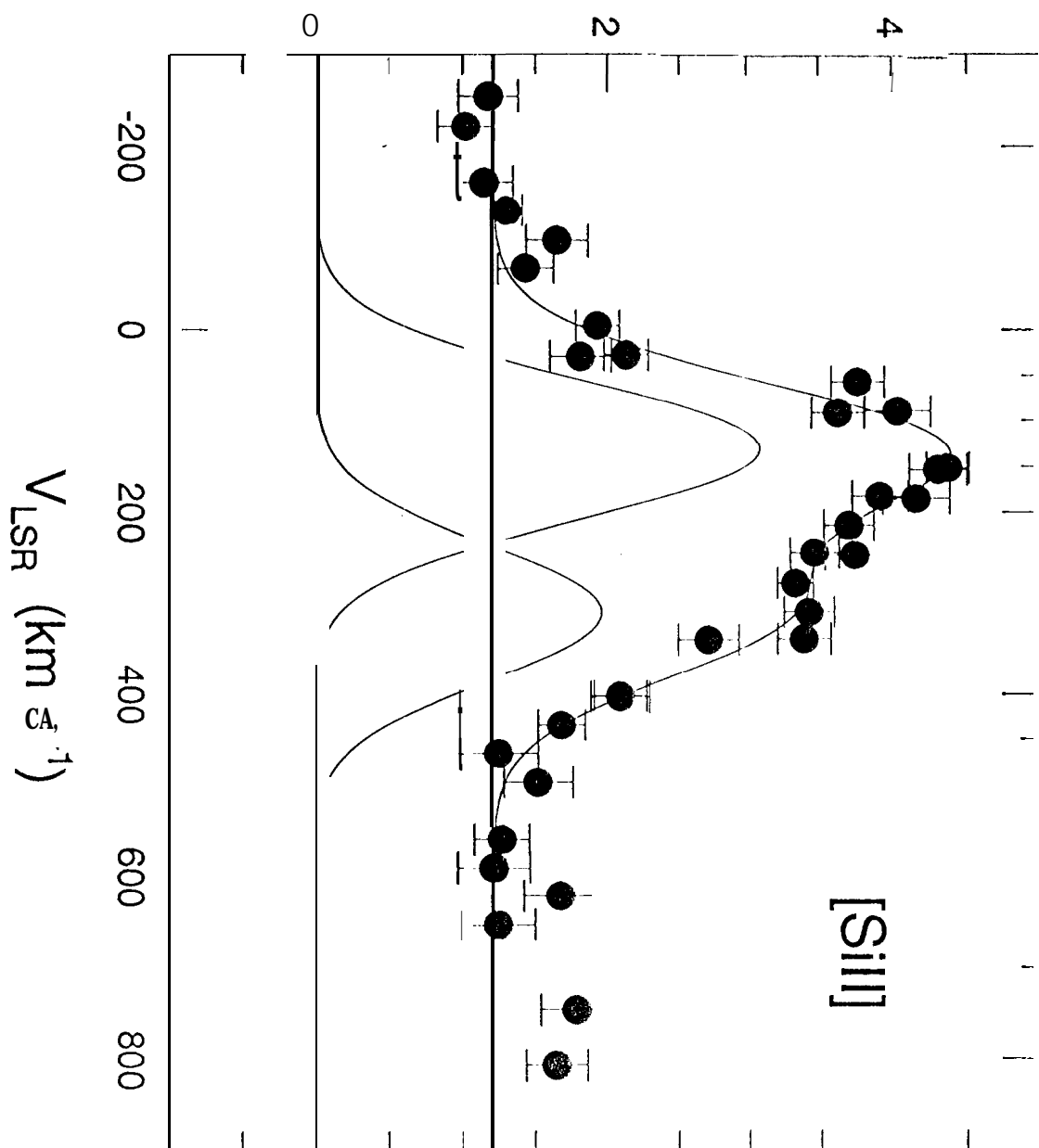
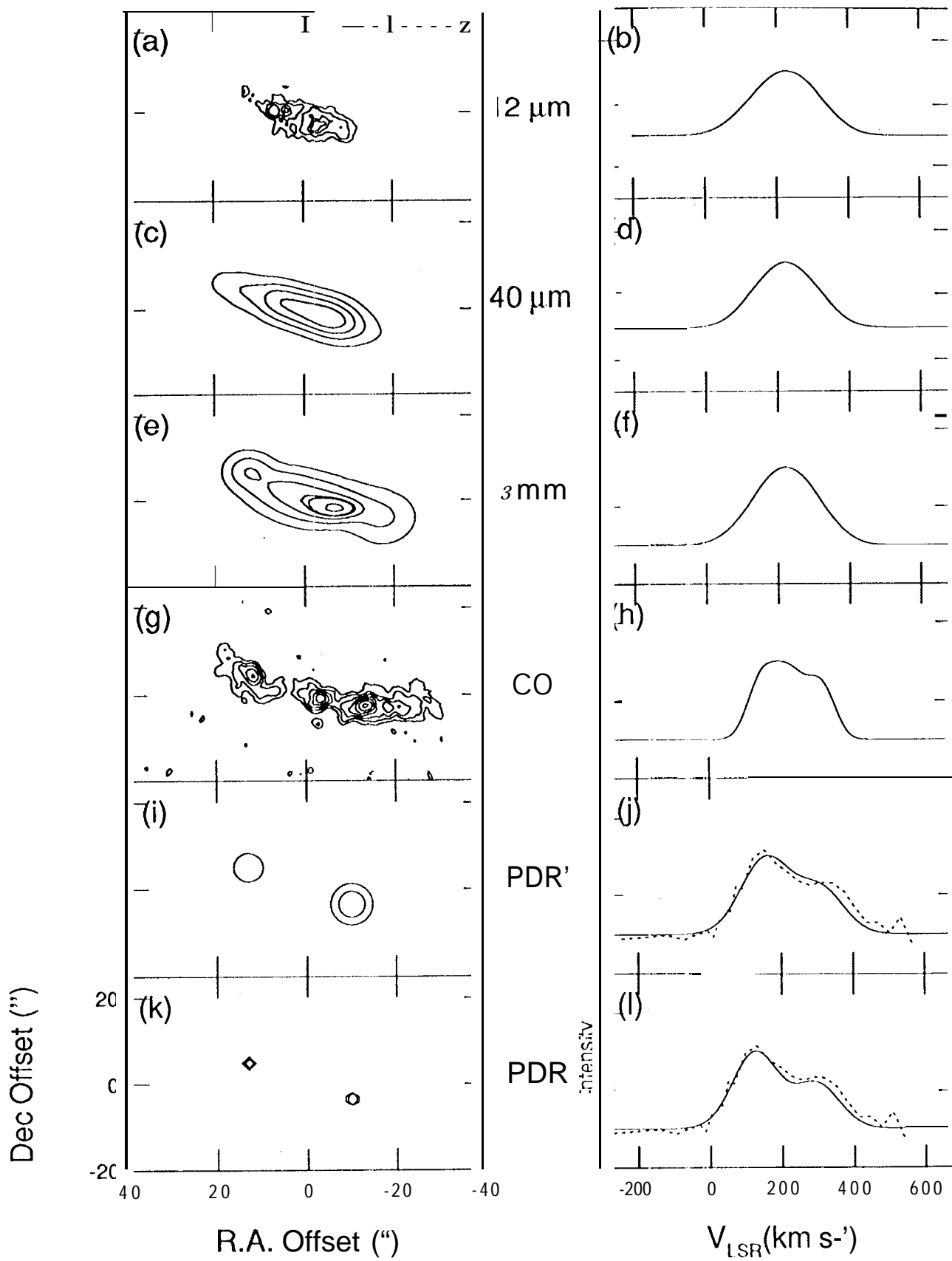


Fig 6b



ⁿ
fig 7